Electronic Research Archive

https://www.aimspress.com/journal/era

ERA, 34(5): 3380–3409.
DOI: 10.3934/era.2026152
Received: 22 February 2026
Revised: 28 March 2026
Accepted: 08 April 2026
Published: 20 April 2026

Research article

Optimal regional control of a spatial diffusion Cholera model with environmental pathogen transmission

Jinghan Hui[†], **Tong Chen**[†] **and Peng Wu**[*]

School of Sciences, Hangzhou Dianzi University, Hangzhou 310018, China

† The authors contributed equally to this work.

* **Correspondence:** Email: hzpengwu89@hdu.edu.cn.

Abstract: In this paper, we propose a regional control strategy to address the challenge of cholera transmission, which is characterized by significant spatial heterogeneity due to its waterborne nature. A spatiotemporal dynamic model was formulated using reaction-diffusion equations, coupled with a four-dimensional optimal control framework encompassing awareness education, expanded vaccination, water chlorination, and treatment. The core mathematical analysis proceeded in three stages: First, the well-posedness of the state system was established, proving the existence and uniqueness of strong solutions. Second, the existence of an optimal control solution was rigorously demonstrated using the method of minimizing sequences. Finally, the first-order necessary optimality conditions were derived by constructing an adjoint system and applying Pontryagin's maximum principle, which explicitly characterized the optimal control quadruple. Numerical simulations validated the theoretical framework, with direct comparisons between regional and uniform control strategies demonstrating the distinct advantage of our approach in cost-effectiveness and outbreak containment efficacy.

Keywords: cholera; reaction-diffusion model; optimal regional control; environmental pathogen transmission

1. Introduction

Cholera, caused by toxigenic *Vibrio cholerae*, is a highly contagious intestinal disease posing a devastating threat to regions lacking safe water and sanitation. Untreated cases can progress to severe dehydration due to acute secretory diarrhea within 24 hours, with a case fatality rate (CFR) as high as 25–50% [1]. Since its first documented global pandemic in 1817 [2], cholera has triggered seven intercontinental pandemics. The seventh pandemic, originating in Indonesia in 1961, is ongoing [3]. The Global Burden of Disease Study estimates that endemic countries experience 2.9 million infections

annually, with approximately 130 million people residing in high-risk communities [4]. The 2022–2023 period witnessed a catastrophic escalation of outbreaks: The World Health Organization (WHO) reported a 175% increase in cases compared to the 2017–2021 average, with 45 countries reporting ongoing transmission. Notably, Yemen reported over 110,000 cases (January–October 2023), and Malawi experienced its highest caseload in 30 years [5]. Mortality is severely underestimated; modeling studies indicate that the underreporting rate may reach 29 times the official death toll [6].

Given the substantial and escalating public health burden of cholera, developing effective prevention and control strategies is crucial. Mathematical models, powerful tools for understanding infectious disease transmission dynamics and optimizing interventions, have long been widely applied in cholera research and have long been extensively employed in the study of infectious disease dynamics. Research on the mathematical modeling of cholera commenced in the 1970s. Capasso and Paveri-Fontana [7] pioneered the construction of an Ordinary Differential Equation (ODEs) model. By establishing the relationship between bacterial concentration in aquatic environments (B in water) and the human infection rate, they revealed the core mechanism of environmental transmission. However, this model neglected spatial heterogeneity and consequently failed to explain the pattern of epidemic propagation along hydrological networks [8]. Subsequently, Codeço [9] built upon this ODEs framework by incorporating environmental reservoir dynamics, thereby emphasizing the persistent role of aquatic environments as bacterial reservoirs.

In 2018, Zhao et al. [10] further extended the ODE framework to develop a complex model incorporating nonlinear incidence rates, multiple transmission pathways (human-to-human/environment-to-human), and imperfect vaccination (efficacy $1 - \sigma$). This model demonstrated that environmental transmission predominates (accounting for $> 85\%$ of transmission) and that insufficient vaccine efficacy may trigger secondary outbreaks. Nevertheless, such models remain constrained by the "homogeneous system" assumption. Although the model by Zhao et al. [10] integrated multiple interacting factors, it did not account for the directional driving force of rivers on bacterial dispersal, rendering it incapable of quantifying geographic risk gradients.

The fundamental limitations of traditional ODEs models have become increasingly apparent. On one hand, models (e.g., Mukandavire et al. [11]) struggle to capture the influence of river flow velocity on transmission directionality: Neglecting spatial heterogeneity in the Zimbabwe epidemic led to a 40% underestimation of propagation speed. On the other hand, control strategies based on homogeneity assumptions (e.g., vaccine optimization by Tian et al. [12]) result in suboptimal resource allocation, whereas riverside communities face infection risks up to 3 times higher than inland areas; such models recommend uniform resource deployment across the region [11]. Experiments further confirmed that *Vibrio* adheres to algae and migrates with water flow [12]. ODEs models lack diffusion terms and are thus unable to investigate such hydro-biological coupling mechanisms. In recent years, reaction-diffusion cholera models for infectious diseases have received considerable attention [13–20]. However, despite the success of these reaction-diffusion models in quantifying the influence of hydrological factors on transmission, the design of control strategies predominantly relies on uniform control strategies across the domain. Given cholera's distinct pattern of regional endemicity and outbreaks concentrated along river networks, implementing traditional full-space control measures, such as mass vaccination or basin-wide disinfection, is extremely challenging and inefficient in resource-limited settings. Empirical evidence indicates that a uniform resource allocation strategy requires 3.2 times the medical resources compared to regional control to achieve

equivalent containment efficacy (based on recalibration of Wang et al. [13]). More critically, uniform control may exacerbate transmission heterogeneity: When resources are dispersed into low-risk areas, riverside communities may experience exponential outbreaks due to insufficient intervention, with model simulations showing that the basic reproduction number R_0 can surge sharply by up to 47% [9].

Consequently, we move away from the traditional uniform control framework. Given the practical dilemmas of limited budgets and medical resources, implementing peak-intensity interventions is often infeasible. Optimal control theory addresses these challenges by providing a rigorous mathematical framework to derive spatially and temporally optimized trajectories [21,22], ensuring that public health benefits are maximized within the bounds of constraints. Building upon this rationale, we establish, for the first time, a regional optimal control model based on reaction-diffusion equations to identify high-risk zones and optimize intervention efficiency. This approach identifies high-risk zones (such as river confluences and densely populated areas) for targeted interventions, thereby maximizing control efficiency. In this paper, we establish a reaction-diffusion regional optimal control model for cholera, aiming to investigate the impact of regional control strategies on cholera transmission dynamics. Furthermore, utilizing COMSOL Multiphysics and MATLAB in conjunction with demographic and geographic data from a specific location, we conduct spatiotemporal visualization of the disease spread.

The remainder of the paper is structured as follows: In Section 2, we formulate the reaction-diffusion regional optimal control model for cholera. In Section 3, we provide a proof for the existence of strong solutions. In Section 4, we derive and prove the existence of an optimal solution. In Section 5, we present numerical simulations; through controlled variable comparisons, we demonstrate the superiority of regional control over conventional control and examine the influence of varying initial distributions on control efficacy. Finally, in Section 6, we conclude the paper.

2. Model formulation

While developing the model, the population is divided into four classes: The susceptible, the vaccinated, the infected, and the recovered, whose numbers at the time t are $S(t)$, $V(t)$, $I(t)$, and $R(t)$ [1], respectively. Moreover, the concentrations of *Vibrio cholerae* at time t are denoted by $P(t)$. Susceptible individuals are recruited at a constant rate Λ. The susceptible is infected with a general incidence $h(S, I)$ by infectious individuals and by vibrios at the rate $f(S, P)$. The host has a natural death rate μ. Furthermore, the susceptible is vaccinated at the rate ϕ. On the one hand, the vaccine disappears at rate η. However, the imperfect vaccine enables breakthrough infections in vaccinated individuals through contact with infected individuals, with transmission scaled by a factor σ relative to susceptible individuals. Parameter σ in [0,1], represents the efficacy of a vaccine. Specifically, $0 < \sigma < 1$ signifies that the vaccine's efficacy is less than 100%, meaning it does not completely prevent infection. When $\sigma = 0$, it indicates that the vaccine is 100% effective in inhibiting the infection. Conversely, $\sigma = 1$ denotes that the vaccine has no efficacy, implying that it fails to provide any protection against infection. Infected individuals recover at a rate denoted by γ, assuming that recovery confers permanent immunity within the timeframe of a short-term outbreak. In addition to the natural mortality rate, the disease imparts an additional mortality rate to the infected individuals, expressed as δ_I. Initially, the infected subjects release vibrios into the aquatic environment at a rate ξ. Then vibrios lose viability at the rate δ.

The high pathogen shedding rate ($\xi = 10^{13}$/hour) and environmental persistence (δ) necessitate

targeted interventions to break the transmission cycle. We adopt a four-dimensional control strategy (u_1–u_4) to combat cholera transmission, with the following biological rationale: We use u_1–u_4 as the basic four control measures, where u_1 is the awareness education control measure, u_2 is the expanded vaccination control measure, u_3 is the water chlorination control measure, and u_4 is the treatment of infected individuals control measure. Awareness education serves as the cornerstone of the prevention system. *V. cholerae* can diffuse over long distances through freshwater ecosystems [23], and when residents lack protective awareness, disinfected water bodies can be recontaminated [23]. Therefore, through u_1, we implement behavioral interventions such as safe water storage and proper handwashing to reduce "human-water" contact risks at the source, establishing a behavioral foundation for subsequent measures. However, behavioral change requires long-term reinforcement [23], while cholera outbreaks exhibit exponential growth (with patient bacterial shedding rates as high as 10^{13} per hour, [24]). Thus, u_2 Expanded Vaccination must be simultaneously initiated; oral vaccines provide dual protection: Short-term coverage during the incubation period, while herd immunity extends the prevention cycle [25]. This approach rapidly constructs an immune barrier during the early epidemic phase, compensating for the latency in u_1 behavioral interventions.

However vaccines require 7–14 days to establish effective immunity, and extreme weather events (floods/droughts) can cause recurrent water contamination [23]. Therefore, u_3 Water Chlorination is introduced: Through chemical inactivation of aquatic vibrios [26], the core transmission chain of aquatic vibrios is severed. This measure immediately reduces household drinking water risks, bridges the u_2 immunity gap, and is particularly suitable for river-diffused epidemics [20, 23].

Notably, the protective effect of u_3 on water bodies is transient, as untreated patients continuously discharge high pathogen loads [24] that can exceed environmental disinfection thresholds. Hence, u_4 Treatment functions as the terminal control measure: Through rehydration therapy to rapidly shorten the patient shedding period [27], fecal vibrio concentrations are reduced by a hundredfold within 24 hours. This blocks environmental recontamination at the infection source, ensuring sustainable efficacy of u_1-u_3 measures. The biological characteristics of these four-dimensional controls (temporal dynamics, cost sensitivity) directly determine their differential spatial deployment strategies: The selection of spatial implementation scope for cholera control strategies essentially results from the synergistic optimization of three factors: Transmission dynamics, economic cost constraints, and operational feasibility. In the following section, we detail why u_1 adopts full-regional control while u_2–u_4 employ partial-regional control.

First, the implementation scope of full-regional awareness control u_1 covers the entire domain Ω. This necessity stems from the uncontrollable diffusion mechanism of cholera transmission: Pathogens disseminate diffusely through contaminated water sources, and population mobility distributes exposure risks indiscriminately across space. Moreover, full-regional education synchronously modifies resident water-sanitation behaviors, effectively suppressing the environment-to-human transmission function $f(S, P)$ and human-to-human transmission function $h(S, I)$. This builds a fundamental prevention barrier, enabling full-domain risk suppression through low-cost quadratic terms in the objective function.

In contrast, u_2 expanded vaccination, u_3 water disinfection, and u_4 infected case isolation are strictly confined to epidemic-prone subdomains A. This strategy arises from the significant spatial aggregation observed; infectee density I and pathogen concentration P in outbreak epicenters can be several times higher than in peripheral areas. Moreover, large-scale vaccine procurement and

administration, continuous reagent input for water disinfection, and infrastructure/human resource demands for case isolation incur prohibitively high costs. Therefore, subdomain control utilizes characteristic functions to precisely focus limited resources on core transmission sources: Vaccines prioritize high-transmission-risk zones to avoid inefficiency, water disinfection targets pathogen-enriched water bodies to reduce chemical consumption, and case isolation concentrates on infection density hotspots to minimize redundant facility investment.

2.1. The model without control

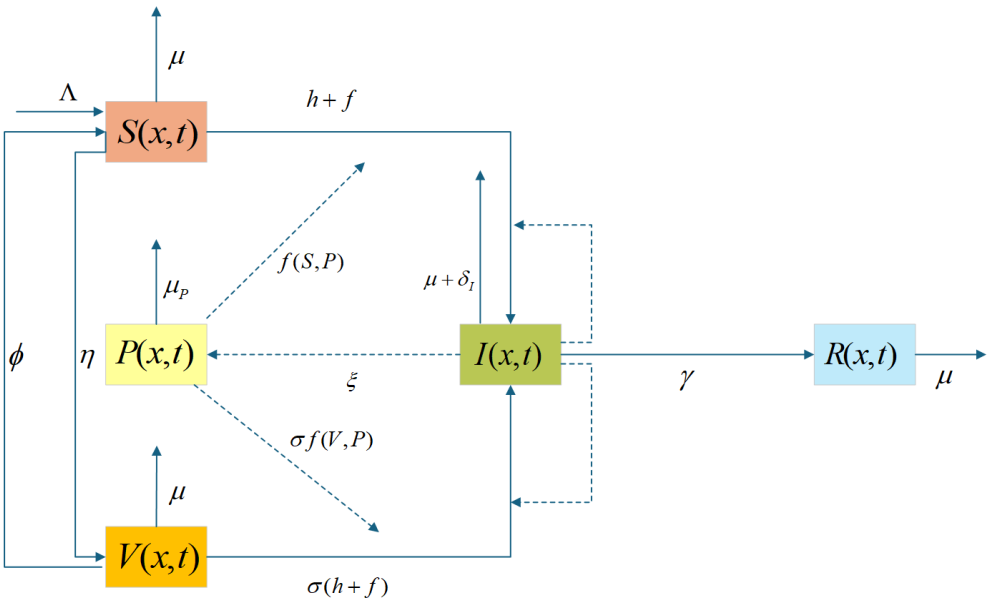

Figure 1. Schematic flow diagram of the cholera model.

We denote by Ω a fixed and bounded domain in $\mathbb{R}^2$ with smooth boundary $\partial\Omega$, $\partial\Omega$ is the outward unit normal vector on the boundary, and D_S, D_V, D_I, D_R, and D_P are the diffusion coefficients for the susceptible, vaccinated, infected, recovered and pathogen concentration, respectively. Based on the conceptual framework illustrated in Figure 1, we obtain the following model

$$
\begin{cases}
\dfrac{\partial S(x,t)}{\partial t} = D_S \Delta S(x,t) + \Lambda - f(S(x,t), P(x,t)) - h(S(x,t), I(x,t)) + \eta V(x,t) \\
\qquad\qquad - (\phi + \mu) S(x,t), & x \in \Omega,\ t \in [0,T], \\
\dfrac{\partial V(x,t)}{\partial t} = D_V \Delta V(x,t) + \phi S(x,t) - \sigma(f(V(x,t), P(x,t)) + h(V(x,t), I(x,t))) \\
\qquad\qquad - (\eta + \mu) V(x,t), & x \in \Omega,\ t \in [0,T], \\
\dfrac{\partial I(x,t)}{\partial t} = D_I \Delta I(x,t) + f(S(x,t), P(x,t)) + h(S(x,t), I(x,t)) \\
\qquad\qquad + \sigma(f(V(x,t), P(x,t)) + h(V(x,t), I(x,t))) - (\gamma + \delta_I + \mu) I(x,t), & x \in \Omega,\ t \in [0,T], \\
\dfrac{\partial R(x,t)}{\partial t} = D_R \Delta R(x,t) + \gamma I(x,t) - \mu R(x,t), & x \in \Omega,\ t \in [0,T], \\
\dfrac{\partial P(x,t)}{\partial t} = D_P \Delta P(x,t) + \xi I(x,t) - \mu_p P(x,t), & x \in \Omega,\ t \in [0,T],
\end{cases}
\tag{2.1}
$$

with homogeneous Neumann boundary conditions

$$
\frac{\partial S(x,t)}{\partial \nu} = \frac{\partial V(x,t)}{\partial \nu} = \frac{\partial I(x,t)}{\partial \nu} = \frac{\partial R(x,t)}{\partial \nu} = \frac{\partial P(x,t)}{\partial \nu} = 0, \qquad x \in \partial\Omega,\ t \in [0,T],
$$

and initial conditions are given by

$$
S(x,0) = S^0, V(x,0) = V^0, I(x,0) = I^0, R(x,0) = R^0, P(x,0) = P^0, \qquad x \in \Omega.
$$

Moreover, from a biological perspective, we assume that:

(*i*) $S(x,0) = S_0 \geq 0, \quad V(x,0) = V_0 \geq 0, \quad I(x,0) = I_0 \geq 0, \quad R(x,0) = R_0 \geq 0,$
$P(x,0) = P_0 \geq 0;$

(*ii*) $\Phi,\ \eta,\ \sigma,\ \gamma,\ \delta_i,\ \mu,\ \mu_p \in L^\infty;$

(*iii*) $\Lambda \geq 0,\ \Phi \geq 0,\ \eta \geq 0,\ \sigma \geq 0,\ \gamma \geq 0,\ \delta_i \geq 0,\ \mu \geq 0,\ \mu_p \geq 0.$

To show the effect of the spatial factor, and the contribution of people's mobility in the transmission of the cholera virus disease in Gabon, we give a simulation of our model. Values taken for the parameters in this simulation are presented in Table 1. In Figures 2 and 3, in the absence of control measures, the cholera outbreak spreads to the entire region.

Table 1. The values of model parameters.

Parameters	Description	Value	Source
ϕ	Rate of waning immunity	$0.01\ \text{day}^{-1}$	[12]
μ	Natural death rate	$5.48 \times 10^{-3}\ \text{day}^{-1}$	[20]
σ	Progression rate from exposed to infectious	$0.1\ \text{day}^{-1}$	[12]
δ_I	Disease-induced death rate	$0.015\ \text{day}^{-1}$	[15]
β_1	Transmission rate	$3 \times 10^{-9}\ \text{day}^{-1}$	[19]
β_2	Transmission rate	$1 \times 10^{-4}\ \text{day}^{-1}$	[19]
Λ	Recruitment rate of susceptible individuals	$3\ \text{day}^{-1}$	Assume
η	Rate of vaccination	$0.005\ \text{day}^{-1}$	[12]
γ	Recovery rate	$0.004\ \text{day}^{-1}$	[15]
ξ	Rate of pathogen production	$100\ \text{cell} \cdot \text{ml}^{-1} \cdot \text{day}^{-1}$	[20, 21, 28, 29]
δ	Pathogen decay rate	$0.003\ \text{day}^{-1}$	Assume
a	Coefficient	10^{-6}	Assume
b	Coefficient	10^{-6}	Assume
D_S	Diffusion coefficient for susceptible individuals	$0.1\ \text{m}^2 \cdot \text{day}^{-1}$	Assume
D_V	Diffusion coefficient for vaccinated individuals	$0.1\ \text{m}^2 \cdot \text{day}^{-1}$	Assume
D_I	Diffusion coefficient for infectious individuals	$0.1\ \text{m}^2 \cdot \text{day}^{-1}$	Assume
D_R	Diffusion coefficient for recovered individuals	$0.1\ \text{m}^2 \cdot \text{day}^{-1}$	Assume
D_P	Diffusion coefficient for pathogen	$0.1\ \text{m}^2 \cdot \text{day}^{-1}$	Assume

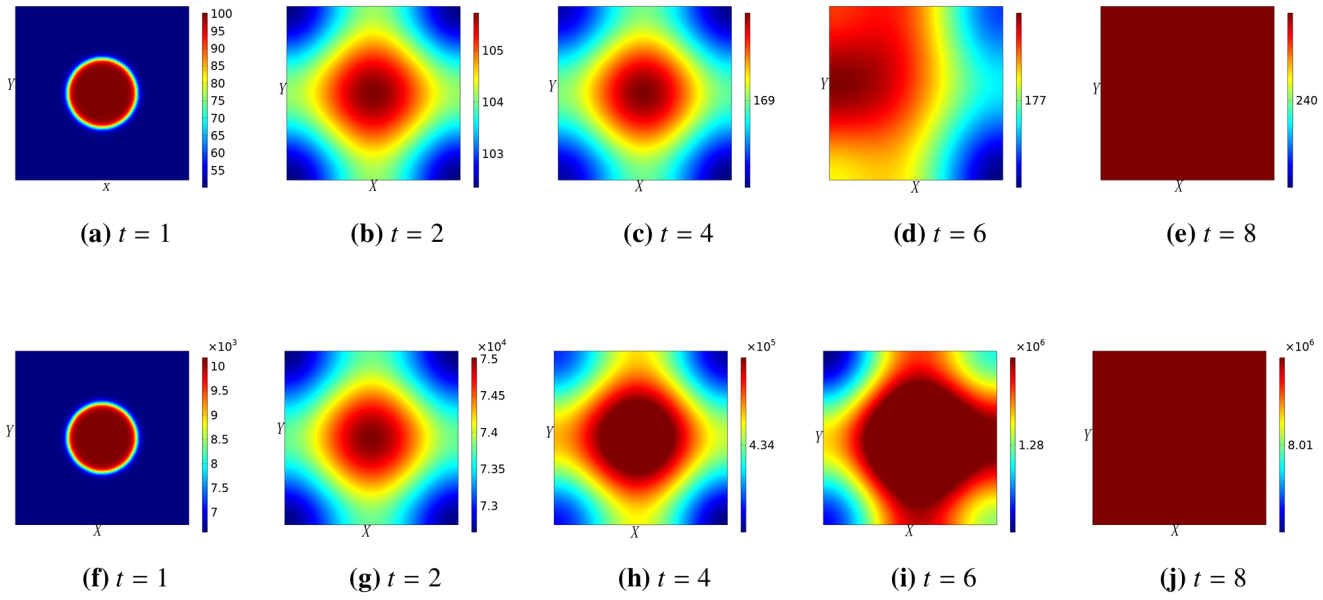

(a) $t = 1$ **(b)** $t = 2$ **(c)** $t = 4$ **(d)** $t = 6$ **(e)** $t = 8$

(f) $t = 1$ **(g)** $t = 2$ **(h)** $t = 4$ **(i)** $t = 6$ **(j)** $t = 8$

Figure 2. Evolution dynamics of I (top row) and P behavior (bottom row) in the middle.

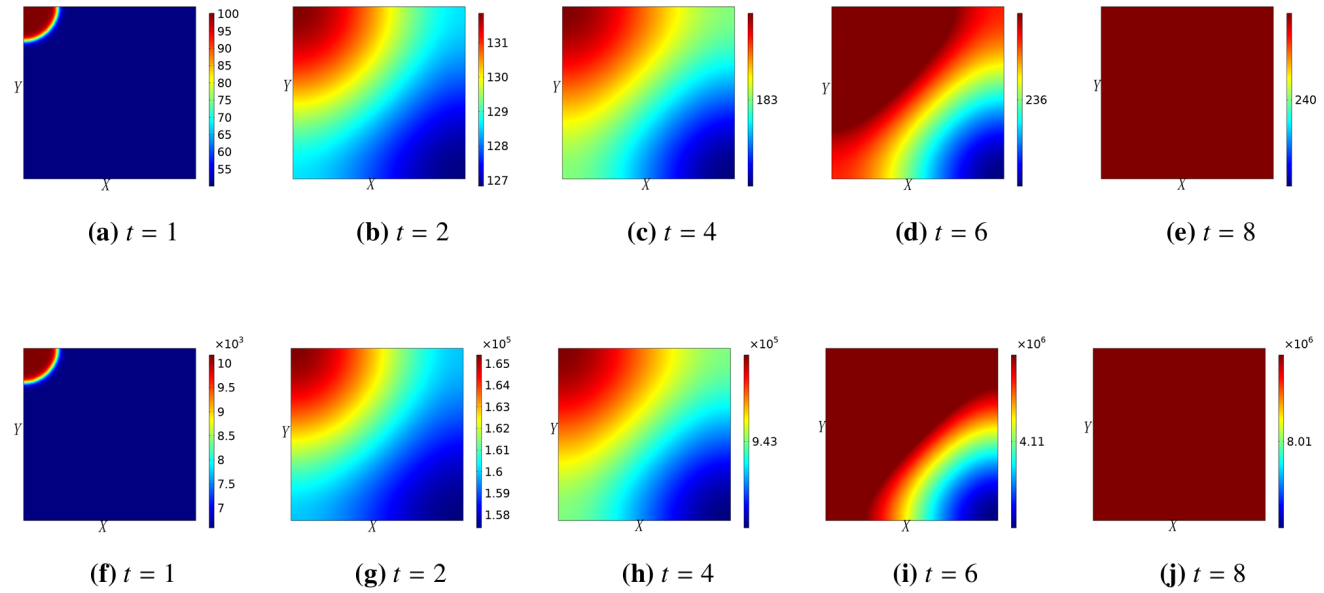

(a) $t = 1$ **(b)** $t = 2$ **(c)** $t = 4$ **(d)** $t = 6$ **(e)** $t = 8$

(f) $t = 1$ **(g)** $t = 2$ **(h)** $t = 4$ **(i)** $t = 6$ **(j)** $t = 8$

Figure 3. Evolution dynamics of I (top row) and P (bottom row) in the top left.

2.2. The model with control

We employ water chlorination u_3 to directly inactivate *V. cholerae* in water bodies within the high-risk subdomain A, thereby severing the environmental transmission chain. In the Dhaka municipal water chlorination study by the researchers in [23], it was found that a free chlorine concentration of 0.1 mg/L was sufficient to inactivate V. cholerae O1, while a concentration of 0.2 mg/L was required to inactivate the O139 serogroup. Therefore, using chlorine tablets and Topaz containers, the intervention households were able to significantly increase the concentration of free chlorine in stored drinking water, effectively inactivating *V. cholerae* and reducing its viability in drinking water.

Through extensive public awareness campaigns, people are informed to stay away from hazardous water sources.Vaccination is introduced at a rate of $u_1(x,t)$ into the susceptible population, so $u_1(x,t)S(x,t)$ are recovered from the susceptible class and moved to the recovered class. In system (2.2), $u_2(x,t)$ represents an expansion of the vaccination coverage applied to individuals within the subdomain $A \subseteq \Omega$. Here, $\chi_A(x)$ denotes the characteristic function of A. Consequently, the term $\chi_A(x)u_2(x,t)I(x,t)$ describes the increase in the implementation of vaccination at the location $x \in A$ at time t, resulting in the transfer of individuals from the susceptible class to the recovered class. In system (2.2), $u_3(x,t)$ represents chlorination of the water source to reduce the concentration of cholera bacteria. within the subdomain $A \subseteq \Omega$. Here, $\chi_A(x)$ denotes the characteristic function of A. CConsequently, the term $\chi_A(x)u_3(x,t)I(x,t)$ describes the active elimination of cholera bacteria at the location $x \in A$ at time t, resulting in a rapid decline in the environmental pathogen concentration. Similarly, in system (2.2), $u_4(x,t)$ represents enhanced medical treatment to accelerate the recovery of infected individuals within the subdomain $A \subseteq \Omega$. Here, $\chi_A(x)$ denotes the characteristic function of A. Consequently, the term $\chi_A(x)u_4(x,t)I(x,t)$ describes the intensified therapeutic intervention applied to infected hosts at the location $x \in A$ at time t, resulting in a rapid decrease in the infected population.

Therefore, we propose the system

$$\begin{cases} \dfrac{\partial S(x,t)}{\partial t} = D_S \Delta S(x,t) + \Lambda - f(S(x,t),P(x,t)) - h(S(x,t),I(x,t)) + \eta V(x,t) \\ \qquad - (\phi+\mu)S(x,t) - u_1(x,t)S(x,t) - \chi_A(x)u_2(x,t)S(x,t),\ x\in\Omega,\ t\in[0,T], \\ \dfrac{\partial V(x,t)}{\partial t} = D_V \Delta V(x,t) + \phi S(x,t) - \sigma(f(V(x,t),P(x,t)) + h(V(x,t),I(x,t))) \\ \qquad - (\eta+\mu)V(x,t) + \chi_A(x)u_2(x,t)S(x,t),\ x\in\Omega,\ t\in[0,T], \\ \dfrac{\partial I(x,t)}{\partial t} = D_I \Delta I(x,t) + f(S(x,t),P(x,t)) + h(S(x,t),I(x,t)) + \sigma(f(V(x,t),P(x,t)) \\ \qquad + h(V(x,t),I(x,t))) - (\gamma+\delta_I+\mu)I(x,t) - \chi_A(x)u_4(x,t)I(x,t),\ x\in\Omega,\ t\in[0,T], \\ \dfrac{\partial R(x,t)}{\partial t} = D_R \Delta R(x,t) + \gamma I(x,t) - \mu R(x,t) + u_1(x,t)S(x,t) + \chi_A(x)u_4(x,t)I(x,t),\ x\in\Omega,\ t\in[0,T], \\ \dfrac{\partial P(x,t)}{\partial t} = D_P \Delta P(x,t) + \xi I(x,t) - \mu_p P(x,t) - \chi_A(x)u_3(x,t)P(x,t),\ x\in\Omega,\ t\in[0,T]. \end{cases} \tag{2.2}$$

The initial conditions and no-flux boundary conditions are given by

$$\begin{cases} \dfrac{\partial S(x,t)}{\partial \nu} = \dfrac{\partial V(x,t)}{\partial \nu} = \dfrac{\partial I(x,t)}{\partial \nu} = \dfrac{\partial R(x,t)}{\partial \nu} = \dfrac{\partial P(x,t)}{\partial \nu} = 0, & x\in\partial\Omega,\ t\in[0,T], \\ S(x,0)=S^0, V(x,0)=V^0, I(x,0)=I^0, R(x,0)=R^0, P(x,0)=P^0, & x\in\Omega. \end{cases} \tag{2.3}$$

Our main objective is to minimize the total number of infected people and to reduce the necessary cost of treatment as well as the cost of chlorination of water. Thus, we have the following objective function

$$\begin{aligned} J((S,I,R,P,V),(u_1,u_2,u_3,u_4)) = &\int_0^T \int_\omega \left[\rho_1 \chi_\omega(x) I(t,x) + \rho_2 \chi_\omega(x) P(t,x)\right] dx\, dt \\ &+ \frac{\sigma_1}{2}\|u_1\|^2_{L^2(Q)} + \frac{\sigma_i}{2}\|u_i\|^2_{L^2([0,T]\times\omega)},\ (i=2,3,4). \end{aligned} \tag{2.4}$$

Subject to systems (2.2)–(2.4), the square of the control variable reflects the severity of side effects of vaccination and treatment, with ρ_1, σ_2, and σ_3 as weight parameters. We define the control set:

$$\begin{aligned} U_{ad} = \{(u_1,u_2,u_3) \in &L^\infty(Q)\times L^\infty([0,T]\times\omega)\times L^\infty([0,T]\times\omega) \mid 0\le u_1\le u_1^{\max}\le 1, \\ &0\le u_2\le u_2^{\max}\le 1, 0\le u_3\le u_3^{\max}\le 1 \text{ and } 0\le u_4\le u_4^{\max}\le 1\}. \end{aligned} \tag{2.5}$$

3. Existence of a strong solution

Theorem 3.1. *The optimal control exists for the problem subject to the reaction-diffusion systems (2.2)–(2.4) under the condition that* $(u_1,u_2,u_3)\in U_{ad}$.

Let $z=(z_1,z_2,z_3,z_4,z_5)=(S,V,I,R,P,S)$, $z^0=\left(z_1^0,z_2^0,z_3^0,z_4^0,z_5^0\right)=(S_0,V_0,I_0,R_0,P_0,S_0)$, $M(\Omega)=\left(L^2(\Omega)\right)^3$, and we will denote A, the linear operator defined by

$$A: D(A)\subset M(\Omega)\longrightarrow M(\Omega), \tag{3.1}$$

where $Az = (\alpha_1\Delta z_1, \alpha_2\Delta z_2, \alpha_3\Delta z_3, \alpha_4\Delta z_4, \alpha_5\Delta z_5) \in D(A), \forall z = (z_1, z_2, z_3, z_4, z_5) \in D(A)$, with the domain of A is defined by

$$D(A) = \left\{ z \in \left(H^2(\Omega)\right)^5, \frac{\partial z_1}{\partial \eta} = \frac{\partial z_2}{\partial \eta} = \frac{\partial z_3}{\partial \eta} = \frac{\partial z_4}{\partial \eta} = \frac{\partial z_5}{\partial \eta} = 0, \text{ a.e } x \in \partial\Omega \right\}. \tag{3.2}$$

We denote by $h(t, x, z(t)) = (h_1(t, x, z), h_2(t, x, z), h_3(t, x, z), h_4(t, x, z), h_5(t, x, z))$ the nonlinear term in (2.2) with

$$\begin{cases} h_1(x, t, z(t)) = \Lambda - f(z_1, z_5) - h(z_1, z_3) + \gamma z_2(t) - (\phi + \mu)z_1(t) - u_1(x, t)z_1(t), \\ h_2(x, t, z(t)) = \phi z_1(t) - \sigma(f(z_2, z_5) + h(z_2, z_3)) - (\eta + \mu)z_2(t) + \chi_A(x)u_2(x, t)z_1(t), \\ h_3(x, t, z(t)) = f(z_2, z_3) + h(z_2, z_3) - (\gamma + \delta_1 + \mu)z_3(t) - \chi_A(x)u_4(x, t)z_3(t), \\ h_4(x, t, z(t)) = \gamma z_3(t) - \mu z_4(t) + u_1(x, t)z_1(t), \\ h_5(x, t, z(t)) = \xi z_3(t) - \mu_p z_5(t) - \chi_A(x)u_3(x, t)z_5(t) + \chi_A(x)u_4(x, t)z_3(t). \end{cases}$$

From a biological perspective, we have the following assumptions hold:

Assumption 3.1. (A1) *$\Omega \subset \mathbb{R}^n$ is a bounded domain with smooth boundary $\partial\Omega$, and $T > 0$ is a fixed terminal time. The space-time cylinder is $Q_T := (0, T) \times \Omega$;*

(A2) *Initial conditions satisfy $S_0, I_0, P_0 \in H^1(\Omega) \cap L^\infty(\Omega)$ with $S_0, I_0, P_0 \geq 0$ and $S_0 + I_0 > 0$ a.e. in Ω;*

(A3) *Model parameters $\beta, \gamma, \sigma, \mu, \delta, \alpha, k$ are positive and bounded: $\beta, \gamma, \sigma, \mu, \delta, \alpha, k \in L^\infty(Q_T)$ with $\beta, \gamma, \sigma, \mu, \delta, \alpha, k \geq 0$;*

(A4) *Diffusion coefficients $d_S, d_I, d_P > 0$ are constants, and the reaction terms satisfy local Lipschitz conditions.*

3.1. Existence and uniqueness of state solutions

Theorem 3.2. *Let $\Omega \subset \mathbb{R}^n$ be a bounded smooth domain, $T > 0$, and initial data $z^0 \in D(A)$ with components $z_i^0 \geq 0$. Assume the controls $(u_1, u_2, u_3, u_4) \in U_{ad}$, where $U_{ad} := \{u \in L^\infty(\Omega \times (0, T)) \mid 0 \leq u_i \leq u_{\max}\}$, and the nonlinear terms f, h satisfy local Lipschitz conditions. Then the reaction-diffusion system: $\partial_t z = Az + h(t, x, z)$, $z(0) = z^0$, where $Az = (\alpha_1\Delta z_1, \ldots, \alpha_5\Delta z_5)$, admits a unique strong solution: $z \in W^{1,2}([0, T]; \mathcal{M}(\Omega)) \cap L^2(0, T; D(A))$.*

Proof. Let $A = \text{diag}\{\alpha_1\Delta, \ldots, \alpha_5\Delta\}$ with Neumann boundary conditions. Since A generates an analytic semigroup $\{e^{At}\}_{t\geq 0}$ on $\Omega = (L^2(\Omega))^5$, and the nonlinearity $h(t, x, z)$ composed of reaction and control terms, is locally Lipschitz in z uniformly in (t, x), by assumption, we apply the standard semigroup theory for semilinear evolution equations. There exists $T_0 > 0$ such that the initial value problem $\partial_t z = Az + h(t, x, z), \quad z(0) = z^0$, admits a unique strong solution $z \in C([0, T_0]; D(A)) \cap C^1([0, T_0]; \Omega)$.

We establish non-negativity of each component z_i using Stampacchia's method. For $i = 1, \ldots, 5$, define the negative part $z_i^- = \max\{-z_i, 0\}$ and consider the function $H(s) = (s^-)^2$. Multiplying the i-th equation by $-z_i^-$ and integrating over Ω, one has

$$\int_\Omega \partial z_i(-z_i^-)dx = \int_\Omega [\alpha_i\Delta z_i + h_i(t, x, z)](-z_i^-)dx \tag{3.3}$$

$$= -\alpha_i \int_\Omega |\nabla z_i^-|^2 dx + \int_\Omega h_i(t, x, z)(-z_i^-)dx \leq L \int_\Omega |z_i^-|^2 dx, \tag{3.4}$$

where we used Green's formula with Neumann condition $\partial_\eta z_i|_{\partial\Omega} = 0$, and the Lipschitz condition $|h_i(t,x,z)| \le L|z|$. This yields $\frac{1}{2}\frac{d}{dt}z_{iL^2(\Omega)}^{-2} \le Lz_{iL^2(\Omega)}^{-2}$. Since $z_i^-(0,x) = 0$ by $z_i^0 \ge 0$, and Gronwall's inequality implies $z_i^-(t,x) = 0$ for all $t \in [0,T_0]$. Hence, $z_i(t,x) \ge 0$ on $[0,T_0]\times\Omega$. Denote $M(t) = \int_\Omega [S(t,x) + V(t,x) + I(t,x) + R(t,x)]dx$. Differentiating and using the boundedness of controls $u_i \in [0,u_{\max}]$:

$$\begin{aligned}\frac{dM}{dt} &= \int_\Omega [-\beta S I + \mu_V V + \mu_R R - \delta I + u_1 S - u_2 I]dx \\ &\le C_1 M(t) + C_2\|\Omega\|u_{\max}.\end{aligned}$$

By Gronwall's inequality, one has $M(t) \le (M(0) + C_2\|\Omega\|u_{\max}T)e^{C_1T} := K(T)$. For pathogens P, the equation: $\partial P = d_P\Delta P + \gamma I - \mu_P P - u_3 P$ with $I \le K(T)$ and $u_3 \ge 0$ implies: $P_{L^\infty(Q_{T_0})} \le C(T)P^0_{L^\infty} + \frac{\gamma K(T)}{\mu_P}$. These uniform bounds imply that h satisfies a global Lipschitz condition, enabling unique extension to $[0,T]$. The solution $z \in L^2(0,T;D(A))$ satisfies $\partial z - Az = h \in L^2$. Since $|h(t,x,z)| \le C(1+|z|)$ and $z \in L^\infty$, we use L^2-maximal regularity for sectorial operators $\partial_t z_{L^2} + Az_{L^2} \le C(h_{L^2} + z^0_{D(A)})$. This implies the enhanced regularity: $z \in W^{1,2}([0,T];\Omega) \cap L^2(0,T;D(A))$. Uniqueness follows from continuous dependence on initial data under the Lipschitz condition.

3.2. Solution properties

Theorem 3.3. *Under the 3.1, the strong solution z satisfies: The solution is non-negative: $z_i(t,x) \ge 0$ for all $(t,x) \in Q := (0,T)\times\Omega$ and $i = 1,\dots,5$. It is uniformly bounded: $\|z_i\|_{L^\infty(Q)} \le C(T)$ for all $i = 1,\dots,5$, where $C(T)$ depends on T and initial data. Regularity estimates hold:*

$$\sum_{i=1}^{5}\left(\|\partial_t z_i\|_{L^2(Q)} + \|z_i\|_{L^2(0,T;H^2(\Omega))} + \|z_i\|_{L^\infty(0,T;H^1(\Omega))}\right) \le C$$

with constant C independent of t.

Proof. Assume by contradiction that some z_i becomes negative. We define the auxiliary function $w_i = e^{-\lambda t}z_i$ for sufficiently large $\lambda > 0$. From the reaction-diffusion system in Theorem 3.1:

$$\partial_t w_i - d_i\Delta w_i = e^{-\lambda t}f_i(z) - \lambda w_i, \tag{3.5}$$

where f_i is the reaction term. By 3.1, f_i satisfies $f_i(z) \ge -K\sum_{j=1}^5 z_j$ when $z_i = 0$. Choosing $\lambda > 5K$, one gets $\partial_t w_i - d_i\Delta w_i \ge -K\sum_{j\ne i} w_j - (\lambda - K)w_i \ge -5K\|w\|_\infty - (\lambda - K)w_i$.

If w_i first becomes negative at (t_0,x_0), then $\partial_t w_i \le 0$, $\quad -\Delta w_i \le 0$, $\quad w_i = 0$, $\quad w_j \ge 0$ $\quad (j \ne i)$. Thus, the left-hand side < 0, but the right-hand side > 0, which is a contradiction. Hence, $w_i \ge 0$, implying $z_i > 0$. We define the total mass $V(t) = \sum_{i=1}^5 \int_\Omega z_i\,dx$. From Theorem 3.1's hypotheses, the reaction terms satisfy

$$\sum_{i=1}^{5} f_i(z) \le L\sum_{i=1}^{5} z_i + M. \tag{3.6}$$

Integrating the PDEs system over Ω, we have $\frac{d}{dt}V(t) = \sum_{i=1}^5 \int_\Omega f_i(z)\,dx \le LV(t) + M|\Omega|$. Then, by Gronwall inequality, one has $V(t) \le e^{Lt}V(0) + \frac{M|\Omega|}{L}(e^{Lt} - 1)$. Since the non-negativity, $\|z_i(t)\|_{L^1(\Omega)} \le V(t)$. Using the L^1–L^∞ smoothing of parabolic systems yields

$$\|z_i\|_{L^\infty(Q)} \le C_1(T)\left(1 + \sup_{t\in[0,T]} V(t)\right) \le C(T). \tag{3.7}$$

Multiplying the $\partial_t z_i - d_i\Delta z_i = f_i(\mathbf{z})$ by $-\Delta z_i$ and integrating over Ω, we obtain

$$\int_\Omega \partial_t z_i(-\Delta z_i)dx + d_i\int_\Omega |\Delta z_i|^2 dx = -\int_\Omega f_i(z)\Delta z_i dx.$$

Then, by Green's theorem and uniform boundedness ($|f_i(z)| \le K$), we have

$$\frac{1}{2}\frac{d}{dt}\|\nabla z_i\|^2_{L^2(\Omega)} + d_i\|\Delta z_i\|^2_{L^2(\Omega)} \le K\|\Delta z_i\|_{L^1(\Omega)} \le \frac{d_i}{2}\|\Delta z_i\|^2_{L^2(\Omega)} + \frac{K^2|\Omega|}{2d_i}.$$

Summing over i and integrating on $[0, T]$, one has

$$\sup_{t\in[0,T]}\sum_{i=1}^{5}\|\nabla z_i(t)\|^2_{L^2(\Omega)} + \sum_{i=1}^{5}\int_0^T \|\Delta z_i\|^2_{L^2(\Omega)}dt \le C_1.$$

Then, $\|\partial_t z_i\|_{L^2(Q)} \le \|d_i\Delta z_i\|_{L^2(Q)} + \|f_i(z)\|_{L^2(Q)} \le C_2$. Combining (3.5)–(3.7), we obtain

$$\sum_{i=1}^{5}\left(\|\partial_t z_i\|_{L^2(Q)} + \|z_i\|_{L^2(0,T;H^2(\Omega))} + \|z_i\|_{L^\infty(0,T;H^1(\Omega))}\right) \le C.$$

Theorem 3.4. *Consider the controlled reaction-diffusion system (2.2) with Neumann boundary conditions and initial data* $(S^0, V^0, I^0, R^0, P^0) \ge 0$. *Assume (3.1). Then there exist optimal controls* $(u_1^*, u_2^*, u_3^*, u_4^*)$ *and states* $(S^*, V^*, I^*, R^*, P^*)$, *minimizing:*

$$J(u) = \int_0^T\int_\Omega\left[I(x,t) + \frac{\sigma_1}{2}u_1^2 + \frac{\sigma_2}{2}u_2^2 + \frac{\sigma_3}{2}u_3^2 + \frac{\sigma_4}{2}u_4^2\right]dxdt.$$

Proof. Let $\{u_n\} = (u_{1,n}, u_{2,n}, u_{3,n}, u_{4,n})$ be a minimizing sequence in U_{ad}, and $(S_n, V_n, I_n, R_n, P_n)$ the corresponding solutions. By Theorems 3.1 and 3.2, we establish

(i) Non-negativity and L^∞ bounds: Solutions satisfy $S_n, V_n, I_n, R_n, P_n \ge 0$ a.e. in $Q = \Omega\times[0,T]$. Then, there exists $C > 0$ independent of n such that

$$\|S_n\|_{L^\infty(Q)} + \|V_n\|_{L^\infty(Q)} + \|I_n\|_{L^\infty(Q)} + \|R_n\|_{L^\infty(Q)} + \|P_n\|_{L^\infty(Q)} \le C.$$

(ii) Proof sketch: Construct super-solutions $\bar{S} = \|S^0\|_{L^\infty} + \Lambda T e^{\mu t}$, $\bar{P} = \|P^0\|_{L^\infty} + \xi\|\bar{I}\|Te^{\mu_p t}$, and apply comparison principles to each equation.

(iii) $L^2(0,T;H^1(\Omega))$ estimates: Multiply each equation by its state variable and integrate over Ω. Using Young's inequality and Lipschitz continuity

$$\frac{1}{2}\frac{d}{dt}\|S_n\|^2_{L^2} + D_S\|\nabla S_n\|^2_{L^2} \le C\left(1 + \|S_n\|^2_{L^2} + \|V_n\|^2_{L^2} + \|I_n\|^2_{L^2} + \|P_n\|^2_{L^2}\right),$$
$$\frac{1}{2}\frac{d}{dt}\|P_n\|^2_{L^2} + D_P\|\nabla P_n\|^2_{L^2} \le C\left(1 + \|I_n\|^2_{L^2} + \|P_n\|^2_{L^2}\right).$$

Summing all inequalities and applying Gronwall's lemma yields

$$\|S_n\|_{L^2(0,T;H^1)} + \|V_n\|_{L^2(0,T;H^1)} + \|I_n\|_{L^2(0,T;H^1)} + \|R_n\|_{L^2(0,T;H^1)} + \|P_n\|_{L^2(0,T;H^1)} \le C. \tag{3.8}$$

Treat the elliptic part $-\Delta$ using maximal regularity:

$$\|\Delta S_n\|_{L^2(Q)} \le C\left(\left\|\frac{\partial S_n}{\partial t}\right\|_{L^2(Q)} + \|S_n\|_{L^2(Q)} + \|f(S_n, P_n)\|_{L^2(Q)} + \|u_{1,n}S_n\|_{L^2(Q)}\right) \le C, \tag{3.9}$$

where the right-hand side is bounded by (i)-(ii) and U_{ad} constraints. Thus,

$$\|S_n\|_{L^2(0,T;H^2)} + \|V_n\|_{L^2(0,T;H^2)} + \|I_n\|_{L^2(0,T;H^2)} + \|R_n\|_{L^2(0,T;H^2)} + \|P_n\|_{L^2(0,T;H^2)} \le C. \tag{3.10}$$

Directly from the equations and estimates (i)–(iii), we obtain

$$\left\|\frac{\partial S_n}{\partial t}\right\|_{L^2(Q)} \le \|D_S \Delta S_n\|_{L^2} + \|\text{reaction terms}\|_{L^2} \le C. \tag{3.11}$$

Similarly for $\partial_t V_n, \partial_t I_n, \partial_t R_n, \partial_t P_n$. We apply the Aubin-Lions lemma with the embeddings $H^2(\Omega) \Subset H^1(\Omega) \hookrightarrow L^2(\Omega), L^2(0,T;H^2) \cap W^{1,2}(0,T;L^2) \Subset L^2(Q)$. Extract a subsequence (still denoted by n) such that Strong convergence in $L^2(Q)$ $S_n \to S^*$, $V_n \to V^*$, $I_n \to I^*$, $R_n \to R^*$, $P_n \to P^*$ in $L^2(Q)$. Weak convergence in $L^2(0,T;H^2(\Omega))$, we have

$$S_n \rightharpoonup S^*,\ V_n \rightharpoonup V^*,\ I_n \rightharpoonup I^*,\ R_n \rightharpoonup R^*,\ P_n \rightharpoonup P^* \text{ in } L^2(0,T;H^2(\Omega)).$$

The weak convergence of time has

$$\partial_t S_n \rightharpoonup \partial_t S^*,\ \partial_t V_n \rightharpoonup \partial_t V^*,\ \partial_t I_n \rightharpoonup \partial_t I^*,\ \partial_t R_n \rightharpoonup \partial_t R^*,\ \partial_t P_n \rightharpoonup \partial_t P^* \text{ in } L^2(Q).$$

Since U_{ad} is bounded in L^∞, it is bounded in L^2. By weak compactness, it gets $u_{1,n} \rightharpoonup u_1^*$ weakly in $L^2(Q)$, $u_{2,n} \rightharpoonup u_2^*$ weakly in $L^2([0,T]\times A)$, $u_{3,n} \rightharpoonup u_3^*$ weakly in $L^2([0,T]\times A)$, and $u_{4,n} \rightharpoonup u_4^*$ weakly in $L^2([0,T]\times A)$. We verify that $(S^*, V^*, I^*, R^*, P^*)$ satisfies the system with controls $(u_1^*, u_2^*, u_3^*, u_4^*)$. For any test function $\phi \in C_c^\infty(Q)$, the weak convergence has

$$\int_Q \Delta S_n \phi\, dxdt \to \int_Q \Delta S^* \phi\, dxdt \text{ and } \int_Q \frac{\partial S_n}{\partial t}\phi\, dxdt \to \int_Q \frac{\partial S^*}{\partial t}\phi\, dxdt.$$

Similarly for all other linear terms in V_n, I_n, R_n, and P_n, by Lipschitz continuity of f and h, and strong L^2, convergence of states has $\|f(S_n,P_n) - f(S^*,P^*)\|_{L^2(Q)} \le L_f(\|S_n - S^*\|_{L^2} + \|P_n - P^*\|_{L^2}) \to 0$. Analogously, $\|h(S_n,I_n) - h(S^*,I^*)\|_{L^2} \to 0$ and $\|\sigma f(V_n,P_n) + \sigma h(V_n,I_n) - \sigma f(V^*,P^*) - \sigma h(V^*,I^*)\|_{L^2} \to 0$. Global control $u_{1,n}S_n$: $u_{1,n} \rightharpoonup u_1^*$ in $L^2(Q)$, $S_n \to S^*$ in $L^2(Q) \implies u_{1,n}S_n \rightharpoonup u_1^* S^*$ in $L^2(Q)$. Then, we have $\chi_A u_{2,n} S_n$ and $\chi_A u_{3,n} P_n$. Since $\chi_A \in L^\infty([0,T]\times A)$, $u_{2,n} \rightharpoonup u_2^*$ in $L^2([0,T]\times A)$, and $S_n \to S^*$ in $L^2(Q)$, it has

$$\int_{[0,T]\times A} \chi_A u_{2,n} S_n \phi\, dxdt \to \int_{[0,T]\times A} \chi_A u_2^* S^* \phi\, dxdt, \quad \forall \phi \in C_c^\infty(Q). \tag{3.12}$$

Analogously, we have $\chi_A u_{3,n} P_n \rightharpoonup \chi_A u_3^* P^*$ in $L^2(Q)$. Neumann conditions are preserved via trace theorem. Initial conditions hold by continuity. Term (A): $I_n \to I^*$ strongly in $L^2(Q) \implies$ (A) $\to \int_0^T \int_\Omega I^* dxdt$. Terms (B), (C), and (D): Squared L^2-norms are weakly lower semi-continuous, which has $\liminf_{n\to\infty} \|u_{i,n}\|^2 \ge \|u_i^*\|^2$, $i = 1,2,3,4$. Combining (3.8)–(3.12), it gets

$$\liminf_{n\to\infty} J(u_n) \ge \int_0^T \int_\Omega I^* dxdt + \sum_{i=1}^3 \frac{\sigma_i}{2}\|u_i^*\|^2 = J(u^*). \tag{3.13}$$

Consequently, the quadruple $(u_1^*, u_2^*, u_3^*, u_4^*)$ constitutes an optimal control.

4. Necessary optimality conditions

Theorem 4.1. *The mapping* $\mathbf{z} : U_{ad} \to W^{1,2}([0,T];L^2(\Omega))^5$ *with* $z_i \in L^2(0,T;H^1(\Omega)) \cap L^\infty(0,T;L^2(\Omega))$ *for* $i = 1,\dots,5$ *is Gâteaux differentiable at* $\mathbf{u}^* = (u_1^*, u_2^*, u_3^*, u_4^*) \in U_{ad}$. *For any direction* $\mathbf{h} = (h_1, h_2, h_3) \in U_{ad}$, *the directional derivative* $\mathbf{z}'(\mathbf{u}^*)\mathbf{h} = \mathbf{Z} = (S', V', I', R', P')$ *is the unique solution in* $W^{1,2}([0,T];L^2(\Omega))^5$ *with* $Z_i \in L^2(0,T;H^1(\Omega)) \cap L^\infty(0,T;L^2(\Omega))$ *of the following system:*

$$
\begin{cases}
\dfrac{\partial S'}{\partial t} = D_S \Delta S' - \dfrac{\partial f}{\partial S}(S^*,P^*)S' - \dfrac{\partial f}{\partial P}(S^*,P^*)P' - \dfrac{\partial h}{\partial S}(S^*,I^*)S' \\
\qquad - \dfrac{\partial h}{\partial I}(S^*,I^*)I' + \eta V' - (\phi+\mu)S' - u_1^* S' - \chi_A u_2^* S' - h_1 S^* - \chi_A h_2 S^*, \\
\dfrac{\partial V'}{\partial t} = D_V \Delta V' + \phi S' - \sigma\Big(\dfrac{\partial f}{\partial S}(V^*,P^*)V' + \dfrac{\partial f}{\partial P}(V^*,P^*)P' \\
\qquad + \dfrac{\partial h}{\partial S}(V^*,I^*)V' + \dfrac{\partial h}{\partial I}(V^*,I^*)I'\Big) - (\eta+\mu)V' + \chi_A u_2^* S' + \chi_A h_2 S^*, \\
\dfrac{\partial I'}{\partial t} = D_I \Delta I' + \dfrac{\partial f}{\partial S}(S^*,P^*)S' + \dfrac{\partial f}{\partial P}(S^*,P^*)P' + \dfrac{\partial h}{\partial S}(S^*,I^*)S' \\
\qquad + \dfrac{\partial h}{\partial I}(S^*,I^*)I' + \sigma\Big(\dfrac{\partial f}{\partial S}(V^*,P^*)V' + \dfrac{\partial f}{\partial P}(V^*,P^*)P' + \dfrac{\partial h}{\partial S}(V^*,I^*)V' \\
\qquad + \dfrac{\partial h}{\partial I}(V^*,I^*)I'\Big) - (\gamma+\delta_I+\mu)I' - \chi_A u_4^* I' - \chi_A h_4 I^*, \\
\dfrac{\partial R'}{\partial t} = D_R \Delta R' + \gamma I' - \mu R' + u_1^* S' + h_1 S^* + \chi_A u_4^* I' + \chi_A h_4 I^*, \\
\dfrac{\partial P'}{\partial t} = D_P \Delta P' + \xi I' - \mu_p P' - \chi_A u_3^* P' - \chi_A h_3 P^* - \rho_2 \chi_\omega P' + \chi_A u_4^* I' + \chi_A h_4 I^*.
\end{cases}
$$

Proof. Let $\varepsilon > 0$ be sufficiently small. Define $\vec{u}^\varepsilon = \vec{u}^* + \varepsilon\vec{h}$, and let $\vec{z}^\varepsilon = (S^\varepsilon, V^\varepsilon, I^\varepsilon, R^\varepsilon, P^\varepsilon)$ be the state solution corresponding to control $\vec{u}^\varepsilon$. Introduce the difference quotient functions: $Z_S^\varepsilon = \frac{S^\varepsilon - S^*}{\varepsilon}, Z_V^\varepsilon = \frac{V^\varepsilon - V^*}{\varepsilon}, Z_I^\varepsilon = \frac{I^\varepsilon - I^*}{\varepsilon}, Z_R^\varepsilon = \frac{R^\varepsilon - R^*}{\varepsilon}, Z_P^\varepsilon = \frac{P^\varepsilon - P^*}{\varepsilon}$. Subtract the state equations for $\vec{u}^*$ from those for $\vec{u}^\varepsilon$ and divide by ε, then one has

$$
\begin{cases}
\dfrac{\partial Z_S^\varepsilon}{\partial t} = D_S \Delta Z_S^\varepsilon - \dfrac{f(S^\varepsilon,P^\varepsilon) - f(S^*,P^*)}{\varepsilon} - \dfrac{h(S^\varepsilon,I^\varepsilon) - h(S^*,I^*)}{\varepsilon} \\
\qquad + \eta Z_V^\varepsilon - (\phi+\mu)Z_S^\varepsilon - \dfrac{u_1^\varepsilon S^\varepsilon - u_1^* S^*}{\varepsilon} - \chi_A \dfrac{u_2^\varepsilon S^\varepsilon - u_2^* S^*}{\varepsilon}, \\
\dfrac{\partial Z_V^\varepsilon}{\partial t} = D_V \Delta Z_V^\varepsilon + \phi Z_S^\varepsilon - \sigma\left(\dfrac{f(V^\varepsilon,P^\varepsilon) - f(V^*,P^*)}{\varepsilon} + \dfrac{h(V^\varepsilon,I^\varepsilon) - h(V^*,I^*)}{\varepsilon}\right) \\
\qquad - (\eta+\mu)Z_V^\varepsilon + \chi_A \dfrac{u_2^\varepsilon S^\varepsilon - u_2^* S^*}{\varepsilon}, \\
\dfrac{\partial Z_I^\varepsilon}{\partial t} = D_I \Delta Z_I^\varepsilon + \dfrac{f(S^\varepsilon,P^\varepsilon) - f(S^*,P^*)}{\varepsilon} + \dfrac{h(S^\varepsilon,I^\varepsilon) - h(S^*,I^*)}{\varepsilon} \\
\qquad + \sigma\left(\dfrac{f(V^\varepsilon,P^\varepsilon) - f(V^*,P^*)}{\varepsilon} + \dfrac{h(V^\varepsilon,I^\varepsilon) - h(V^*,I^*)}{\varepsilon}\right) - (\gamma+\delta_I+\mu)Z_I^\varepsilon, \\
\dfrac{\partial Z_R^\varepsilon}{\partial t} = D_R \Delta Z_R^\varepsilon + \gamma Z_I^\varepsilon - \mu Z_R^\varepsilon + \dfrac{u_1^\varepsilon S^\varepsilon - u_1^* S^*}{\varepsilon}, \\
\dfrac{\partial Z_P^\varepsilon}{\partial t} = D_P \Delta Z_P^\varepsilon + \xi Z_I^\varepsilon - \mu_p Z_P^\varepsilon - \chi_A \dfrac{u_3^\varepsilon P^\varepsilon - u_3^* P^*}{\varepsilon}.
\end{cases}
\tag{4.1}
$$

From the mean value theorem, there exist points (ξ_S, ξ_P) on the segment joining (S^*, P^*) and $(S^\varepsilon, P^\varepsilon)$, (ζ_S, ζ_I) on the segment joining (S^*, I^*) and $(S^\varepsilon, I^\varepsilon)$, (ξ_V, ξ'_P) on the segment joining (V^*, P^*) and $(V^\varepsilon, P^\varepsilon)$, and (ζ_V, ζ'_I) on the segment joining (V^*, I^*) and $(V^\varepsilon, I^\varepsilon)$, such that

$$\begin{aligned}
\frac{f(S^\varepsilon, P^\varepsilon) - f(S^*, P^*)}{\varepsilon} &= \frac{\partial f}{\partial S}(\xi_S, \xi_P) Z_S^\varepsilon + \frac{\partial f}{\partial P}(\xi_S, \xi_P) Z_P^\varepsilon,\\
\frac{h(S^\varepsilon, I^\varepsilon) - h(S^*, I^*)}{\varepsilon} &= \frac{\partial h}{\partial S}(\zeta_S, \zeta_I) Z_S^\varepsilon + \frac{\partial h}{\partial I}(\zeta_S, \zeta_I) Z_I^\varepsilon,\\
\frac{f(V^\varepsilon, P^\varepsilon) - f(V^*, P^*)}{\varepsilon} &= \frac{\partial f}{\partial S}(\xi_V, \xi'_P) Z_V^\varepsilon + \frac{\partial f}{\partial P}(\xi_V, \xi'_P) Z_P^\varepsilon,\\
\frac{h(V^\varepsilon, I^\varepsilon) - h(V^*, I^*)}{\varepsilon} &= \frac{\partial h}{\partial S}(\zeta_V, \zeta'_I) Z_V^\varepsilon + \frac{\partial h}{\partial I}(\zeta_V, \zeta'_I) Z_I^\varepsilon.
\end{aligned}$$

The control terms satisfy

$$\frac{u_1^\varepsilon S^\varepsilon - u_1^* S^*}{\varepsilon} = u_1^\varepsilon Z_S^\varepsilon + h_1 S^\varepsilon, \frac{u_2^\varepsilon S^\varepsilon - u_2^* S^*}{\varepsilon} = u_2^\varepsilon Z_S^\varepsilon + h_2 S^\varepsilon, \frac{u_3^\varepsilon P^\varepsilon - u_3^* P^*}{\varepsilon} = u_3^\varepsilon Z_P^\varepsilon + h_3 P^\varepsilon.$$

Substituting into the difference quotient system, we have

$$\begin{cases}
\dfrac{\partial Z_S^\varepsilon}{\partial t} = D_S \Delta Z_S^\varepsilon - \left[\dfrac{\partial f}{\partial S}(\xi_S, \xi_P) + \dfrac{\partial h}{\partial S}(\zeta_S, \zeta_I)\right] Z_S^\varepsilon - \dfrac{\partial f}{\partial P}(\xi_S, \xi_P) Z_P^\varepsilon - \dfrac{\partial h}{\partial I}(\zeta_S, \zeta_I) Z_I^\varepsilon + \eta Z_V^\varepsilon\\
\qquad\qquad - (\phi + \mu) Z_S^\varepsilon - u_1^\varepsilon Z_S^\varepsilon - \chi_A u_2^\varepsilon Z_S^\varepsilon - h_1 S^\varepsilon - \chi_A h_2 S^\varepsilon,\\
\dfrac{\partial Z_V^\varepsilon}{\partial t} = D_V \Delta Z_V^\varepsilon + \phi Z_S^\varepsilon - \sigma \left[\dfrac{\partial f}{\partial S}(\xi_V, \xi'_P) Z_V^\varepsilon + \dfrac{\partial f}{\partial P}(\xi_V, \xi'_P) Z_P^\varepsilon + \dfrac{\partial h}{\partial S}(\zeta_V, \zeta'_I) Z_V^\varepsilon + \dfrac{\partial h}{\partial I}(\zeta_V, \zeta'_I) Z_I^\varepsilon\right]\\
\qquad\qquad - (\eta + \mu) Z_V^\varepsilon + \chi_A u_2^\varepsilon Z_S^\varepsilon + \chi_A h_2 S^\varepsilon,\\
\dfrac{\partial Z_I^\varepsilon}{\partial t} = D_I \Delta Z_I^\varepsilon + \left[\dfrac{\partial f}{\partial S}(\xi_S, \xi_P) Z_S^\varepsilon + \dfrac{\partial f}{\partial P}(\xi_S, \xi_P) Z_P^\varepsilon + \dfrac{\partial h}{\partial S}(\zeta_S, \zeta_I) Z_S^\varepsilon + \dfrac{\partial h}{\partial I}(\zeta_S, \zeta_I) Z_I^\varepsilon\right]\\
\qquad\qquad + \sigma \left[\dfrac{\partial f}{\partial S}(\xi_V, \xi'_P) Z_V^\varepsilon + \dfrac{\partial f}{\partial P}(\xi_V, \xi'_P) Z_P^\varepsilon + \dfrac{\partial h}{\partial S}(\zeta_V, \zeta'_I) Z_V^\varepsilon + \dfrac{\partial h}{\partial I}(\zeta_V, \zeta'_I) Z_I^\varepsilon\right] - (\gamma + \delta_I + \mu) Z_I^\varepsilon,\\
\dfrac{\partial Z_R^\varepsilon}{\partial t} = D_R \Delta Z_R^\varepsilon + \gamma Z_I^\varepsilon - \mu Z_R^\varepsilon + u_1^\varepsilon Z_S^\varepsilon + h_1 S^\varepsilon,\\
\dfrac{\partial Z_P^\varepsilon}{\partial t} = D_P \Delta Z_P^\varepsilon + \xi Z_I^\varepsilon - \mu_p Z_P^\varepsilon - \chi_A u_3^\varepsilon Z_P^\varepsilon - \chi_A h_3 P^\varepsilon.
\end{cases}$$

We define the linear operator matrix $\mathcal{A} = \mathrm{diag}\{D_S\Delta, D_V\Delta, D_I\Delta, D_R\Delta, D_P\Delta\}$, and the coefficient matrix $\mathcal{H}^\varepsilon(t, x)$ is

$$\mathcal{H}^\varepsilon = \begin{pmatrix}
h_{11}^\varepsilon & h_{12}^\varepsilon & h_{13}^\varepsilon & 0 & h_{15}^\varepsilon\\
h_{21}^\varepsilon & h_{22}^\varepsilon & h_{23}^\varepsilon & 0 & h_{25}^\varepsilon\\
h_{31}^\varepsilon & h_{32}^\varepsilon & h_{33}^\varepsilon & 0 & h_{35}^\varepsilon\\
h_{41}^\varepsilon & 0 & h_{43}^\varepsilon & 0 & 0\\
0 & 0 & h_{53}^\varepsilon & 0 & h_{55}^\varepsilon
\end{pmatrix}.$$

The source term vector is $\mathcal{G}^\varepsilon = (-h_1 S^\varepsilon - \chi_A h_2 S^\varepsilon, \chi_A h_2 S^\varepsilon, 0, h_1 S^\varepsilon, -\chi_A h_3 P^\varepsilon)^\top$. The difference quotient system is $\frac{\partial \vec{Z}^\varepsilon}{\partial t} = \mathcal{A}\vec{Z}^\varepsilon + \mathcal{H}^\varepsilon \vec{Z}^\varepsilon + \mathcal{G}^\varepsilon$. By Theorems 3.1 and 3.2, the state solutions $\vec{z}^\varepsilon, \vec{z}^* \in L^\infty(0, T; L^\infty(\Omega))$ are uniformly bounded, and the partial derivatives are continuous. Thus,

the coefficients of $\mathcal{H}^\varepsilon$ are uniformly bounded in $L^\infty(Q)$. The source term $\mathcal{G}^\varepsilon \in L^\infty(Q)$ is uniformly bounded. To obtain the energy estimates, we take the inner product of the difference quotient system with $\vec{Z}^\varepsilon$ in $L^2(\Omega)$. Applying integration by parts and the homogeneous Neumann boundary conditions, we obtain $\frac{1}{2}\frac{d}{dt}\|\vec{Z}^\varepsilon\|^2_{L^2(\Omega)} + d_{min}\|\nabla\vec{Z}^\varepsilon\|^2_{L^2(\Omega)} \le \int_\Omega(\mathcal{H}^\varepsilon\vec{Z}^\varepsilon\cdot\vec{Z}^\varepsilon + \mathcal{G}^\varepsilon\cdot\vec{Z}^\varepsilon)dx$, where $d_{min} > 0$ is the minimum diffusion coefficient in the operator $\mathcal{A}$. Since the coefficients of $\mathcal{H}^\varepsilon$ are uniformly bounded in $L^\infty(Q)$, the first term on the right-hand side is bounded by $C_1\|\vec{Z}^\varepsilon\|^2_{L^2(\Omega)}$. For the second term, since $\mathcal{G}^\varepsilon$ is uniformly bounded in $L^\infty(Q)$, applying Young's inequality yields $\int_\Omega \mathcal{G}^\varepsilon\cdot\vec{Z}^\varepsilon dx \le \frac{1}{2}\|\vec{Z}^\varepsilon\|^2_{L^2(\Omega)} + C_2$. Combining these estimates gives the differential inequality $\frac{d}{dt}\|\vec{Z}^\varepsilon\|^2_{L^2(\Omega)} + 2d_{min}\|\nabla\vec{Z}^\varepsilon\|^2_{L^2(\Omega)} \le C_3\|\vec{Z}^\varepsilon\|^2_{L^2(\Omega)} + C_4$, where $C_3 = 2C_1 + 1$ and $C_4 = 2C_2$ are positive constants independent of ε. Applying Gronwall's inequality to the above inequality on $[0, T]$, we deduce that $\|\vec{Z}^\varepsilon\|^2_{L^2(\Omega)}$ is uniformly bounded, implying $\vec{Z}^\varepsilon \in L^\infty(0, T; L^2(\Omega))$. Subsequently, integrating the differential inequality with respect to time from 0 to T provides the uniform bound for $\int_0^T \|\nabla\vec{Z}^\varepsilon\|^2_{L^2(\Omega)}dt$. Consequently, there exists a constant $C > 0$ independent of ε such that $\|\vec{Z}^\varepsilon\|_{L^2(0,T;H^1(\Omega))} + \|\vec{Z}^\varepsilon\|_{L^\infty(0,T;L^2(\Omega))} \le C$.

Hence, there exists a subsequence (still denoted by $\vec{Z}^\varepsilon$) and a function $\vec{Z} = (S', V', I', R', P') \in L^2(0, T; H^1(\Omega)) \cap L^\infty(0, T; L^2(\Omega))$ such that $\vec{Z}^\varepsilon \to \vec{Z}$ converges weakly in $L^2(0, T; H^1(\Omega))$. As $\varepsilon \to 0$, $z^\varepsilon \to \vec{z}^*$ converges strongly in $L^2(Q)$ (continuous dependence of state solutions $\frac{\partial f}{\partial S}(\xi_S, \xi_P) \to \frac{\partial f}{\partial S}(S^*, P^*)$), etc., converge strongly in $L^2(Q)$ (continuity of partial derivatives) $u_j^\varepsilon \to u_j^*, S^\varepsilon \to S^*, P^\varepsilon \to P^*$converge strongly in $L^2(Q)$. Taking the limit $\varepsilon \to 0$ in the weak form of the difference quotient equation shows that $\vec{Z}$ satisfies the weak form of the target linear system. By regularity theory, it is a strong solution. In addition, to prove the uniqueness, we suppose $\vec{Z}^{(1)}$ and $\vec{Z}^{(2)}$ are both solutions, and let $\vec{W} = \vec{Z}^{(1)} - \vec{Z}^{(2)}$. Then $\vec{W}$ satisfies the following system:

$$\frac{\partial\vec{W}}{\partial t} = \mathcal{A}\vec{W} + \mathcal{H}^*\vec{W} + \mathcal{G}^\varepsilon, \quad \vec{W}(0, x) = 0, \quad \frac{\partial\vec{W}}{\partial\nu} = 0, \text{ on } \quad [0, T],$$

where $\mathcal{H}^*$ is the matrix with coefficients evaluated at $\vec{z}^*$

$$\mathcal{H}^* = \begin{pmatrix} h_{11}^* & h_{12}^* & h_{13}^* & 0 & h_{15}^* \\ h_{21}^* & h_{22}^* & h_{23}^* & 0 & h_{25}^* \\ h_{31}^* & h_{32}^* & h_{33}^* & 0 & h_{35}^* \\ h_{41}^* & 0 & h_{43}^* & 0 & 0 \\ 0 & 0 & h_{53}^* & 0 & h_{55}^* \end{pmatrix}.$$

To maintain the conciseness and fluency of the main text, the full form of the adjoint matrix H^* is provided in the Appendix. Then we define the energy function

$$E(t) = \frac{1}{2}\int_\Omega \left(W_S^2 + W_V^2 + W_I^2 + W_R^2 + W_P^2\right)dx.$$

Differentiating it with respect to t, we obtain

$$\dot{E}(t) = \sum_i \int_\Omega W_i D_i \Delta W_i dx + \int_\Omega \begin{pmatrix} W_S \\ W_V \\ W_I \\ W_R \\ W_P \end{pmatrix}^\top \mathcal{H}^* \begin{pmatrix} W_S \\ W_V \\ W_I \\ W_R \\ W_P \end{pmatrix} dx.$$

By Green's formula and boundary conditions, we have $\int_\Omega W_i \Delta W_i dx = -\int_\Omega |\nabla W_i|^2 dx \le 0$. Since $\mathcal{H}^*$ is bounded, there exists $K > 0$ such that $\left|\int_\Omega \vec{W}^\top \mathcal{H}^* \vec{W} dx\right| \le K\|\vec{W}\|^2_{L^2(\Omega)} = 2KE(t)$. Thus, $\dot{E}(t) \le 2KE(t)$. By Gronwall's inequality and $E(0) = 0$, we have $E(t) \equiv 0$, so $\vec{W} \equiv 0$. The solution is unique. In conclusion, the mapping $\vec{u} \mapsto \vec{z}(\vec{u})$ is Gâteaux differentiable at $\vec{u}^*$, and the directional derivative is $\vec{Z}$.

Lemma 4.2. *For the optimal state trajectory $z^* = (S^*, V^*, I^*, R^*, P^*)$ and optimal control u^*, there exists a unique solution $p = (p_S, p_V, p_I, p_R, p_P)$ to the linear parabolic system*

$$-\frac{\partial p}{\partial t} - \mathcal{A}p - \mathcal{H}^* p = D\rho,\ t \in [0, T], \tag{4.2}$$

satisfying terminal conditions $p_i(T, x) = 0$ for $i = \{S, V, I, R, P\}$.

Proof. The adjoint system is derived from Pontryagin's maximum principle for distributed parameter systems. $\mathcal{A}$ denotes the reaction terms of the state equations, $D = \begin{pmatrix} 0&0&0&0&0\\ 0&0&0&0&0\\ 0&0&1&0&0\\ 0&0&0&0&0\\ 0&0&0&0&1 \end{pmatrix}$ and $\rho = (0, 0, \rho_1, 0, \rho_2)$. The boundedness of z^* (established in the state system existence theorem) and control constraints ensure coefficients $a_{ij} \in L^\infty(Q_T)$. The diffusion operators $D_i \Delta p_i$ form a uniformly elliptic principal part with positive diffusion coefficients. Homogeneous terminal conditions $p(T) = 0$ and compatible Neumann boundary conditions satisfy the compatibility requirements for parabolic systems.

By standard linear parabolic PDE theory, the coercivity of the elliptic operators, boundedness of coefficients, and compatibility of terminal-boundary conditions guarantee the existence of a unique solution $p \in L^2(0, T; H^1(\Omega)) \cap C([0, T]; L^2(\Omega))$ for domains with a C^2-boundary. The solution's regularity follows from the smoothness of coefficients and boundary data.

Theorem 4.3. *For the optimal control problem with cost functional $J(u)$, the optimal control $u^* = (u_1^*, u_2^*, u_3^*, u_4^*)$ is characterized by:*

$$\begin{cases} u_1^*(t,x) = \min\left\{u_{\max_1}, \max\left\{0, \dfrac{S^*(t,x)[p_S(t,x) - p_R(t,x)]}{\sigma_1}\right\}\right\}, \\ u_2^*(t,x) = \min\left\{u_{\max_2}, \max\left\{0, \dfrac{\chi_A(x) S^*(t,x)[p_S(t,x) - p_V(t,x)]}{\sigma_2}\right\}\right\}, \\ u_3^*(t,x) = \min\left\{u_{\max_3}, \max\left\{0, \dfrac{\chi_A(x) P^*(t,x) p_P(t,x)}{\sigma_3}\right\}\right\}, \\ u_4^*(t,x) = \min\left\{u_{\max_4}, \max\left\{0, \dfrac{\chi_A(x) I^*(t,x)\,[p_I(t,x) - p_R(t,x)]}{\sigma_4}\right\}\right\}, \end{cases}$$

where p solves the adjoint system in Lemma 4.2.

Proof. Define the Hamiltonian functional $(z, u, p) = \rho_1 \chi_\omega I + \sum_{k=1}^3 \frac{\sigma_k}{2} u_k^2 + \sum_i p_i f_i(z, u)$, where $i \in \{S, V, I, R, P\}$ and f_i are the reaction terms of the state equations [30, 31]. The maximum principle requires that at the optimum (z^*, u^*, p) $u_k\big|_{u_k = u_k^*} = 0, k = 1, 2, 3, 4$, almost everywhere in Q_T, subject to control constraints $0 \le u_k \le u_{\max k}$. For control u_1, we have $u_1 = \sigma_1 u_1 + u_1\left[p_S(-u_1 S) + p_R(u_1 S)\right] = \sigma_1 u_1 + S(-p_S + p_R)$. Setting the derivative to zero yields $\sigma_1 u_1^* + S^*(p_R - p_S) = 0 \implies u_1^* = \frac{S^*(p_S - p_R)}{\sigma_1}$.

For control u_2, one has $u_2 = \sigma_2 u_2 + u_2\left[p_S(-\chi_A u_2 S) + p_V(\chi_A u_2 S)\right] = \sigma_2 u_2 + \chi_A S(-p_S + p_V)$, then we get the stationarity condition $\sigma_2 u_2^* + \chi_A S^*(p_V - p_S) = 0 \implies u_2^* = \frac{\chi_A S^*(p_S - p_V)}{\sigma_2}$.

For control u_3, we obtain $u_3 = \sigma_3 u_3 + u_3\left[p_P(-\chi_A u_3 P)\right] = \sigma_3 u_3 - \chi_A P p_P$. Thus, zero derivative implies $\sigma_3 u_3^* - \chi_A P^* p_P = 0 \implies u_3^* = \frac{\chi_A P^* p_P}{\sigma_3}$.

For control u_4, we have $\hat{u}_4 = \frac{\chi_A(x) I^*\left[p_I - p_R\right]}{\sigma_4}$.

To enforce control constraints, we apply the projection operator $u_k^* = \min\left(u_{\max k}, \max(0, \hat{u}_k)\right)$, where $\hat{u}_1 = \frac{S^*(p_S - p_R)}{\sigma_1}$, $\hat{u}_2 = \frac{\chi_A S^*(p_S - p_V)}{\sigma_2}$, $\hat{u}_3 = \frac{\chi_A P^* p_P}{\sigma_3}$ and $\hat{u}_4 = \frac{\chi_A(x) I^*\left[p_I - p_R\right]}{\sigma_4}$. This projection satisfies the necessary optimality conditions

(i) When $\hat{u}_k \in (0, u_{\max k})$, the unconstrained solution holds.

(ii) When $\hat{u}_k \leq 0$, $u_k^* = 0$ implies $u_k \geq 0$.

(iii) When $\hat{u}_k \geq u_{\max k}$, $u_k^* = u_{\max k}$ implies $u_k \leq 0$.

Existence of the optimal control follows from Filippov-Cesari theorem. The explicit characterization satisfies Pontryagin's necessary conditions, and combined with the existence result, constitutes the optimal solution.

5. Numerical simulation

In this section, we perform numerical simulations to demonstrate the behavior of the optimality system, which comprises the coupled state and adjoint equations governed by their respective initial-boundary conditions, terminal conditions, and control characterization. The system is solved through an iterative forward-backward sweep method (FBSM). The state equations are integrated forward in time using the finite element method (FEM) for spatial discretization of the Laplace operator Δ, with simulations implemented in COMSOL Multiphysics software interfaced with MATLAB. The iterative procedure initiates by initializing control variables with predefined estimates. During each forward sweep, state variables are computed at discrete temporal nodes and stored. Subsequently, the adjoint equations are solved backward in time, employing terminal conditions derived from the final state solution while utilizing FEM for spatial discretization. Control variables are updated at each iteration via minimization of the Hamiltonian using the current state-adjoint solution pair. This forward-backward sequence iterates until the relative change in control variables satisfies the convergence criterion

$$\frac{\left\|u^{(k+1)} - u^{(k)}\right\|}{\left\|u^{(k)}\right\|} < \epsilon,$$

where $u^{(k)}$ denotes the control vector at iteration k and ϵ is a prescribed tolerance. The optimal regional control is obtained at convergence. For simplicity, we denote $f(U_1, U_2) = \beta_1 U_1 U_2$ and $h(U_1, U_2) = \beta_2 U_1 U_2$. The spatial domain Ω is considered as a rectangular area with dimensions 1 km $\times$ 1 km and $\chi_A(x, y) := [0.2, 0.8] \times [0.2, 0.8]$. Initial conditions for the compartments are defined as follows:

$$S(x,y) = \begin{cases} 80, & x, y \in \chi_A(x,y), \\ 20, & x, y \notin \chi_A(x,y). \end{cases} \qquad V(x,y) = \begin{cases} 60, & x, y \in \chi_A(x,y), \\ 40, & x, y \notin \chi_A(x,y). \end{cases}$$

$$I(x,y) = \begin{cases} 120, & x, y \in \chi_A(x,y), \\ 50, & x, y \notin \chi_A(x,y). \end{cases} \qquad R(x,y) = \begin{cases} 0, & x, y \in \chi_A(x,y), \\ 0, & x, y \notin \chi_A(x,y). \end{cases}$$

$$P(x,y) = \begin{cases} 10000, & x, y \in \chi_A(x,y), \\ 6500, & x, y \notin \chi_A(x,y). \end{cases}$$

In addition, the upper bounds for the optimal control variables are uniformly set as $u_1^{max} = u_2^{max} = u_3^{max} = u_4^{max} = 1$, with associated constant weight parameters $\rho_1 = 0.1, \rho_2 = 0.001$ and $\sigma_1 = 10, \sigma_2 = 10, \sigma_3 = 50, \sigma_4 = 800$. It should be noted that these simulations are mostly intended to validate the proposed theoretical framework and demonstrate its relative efficacy.

5.1. Validation of regional control strategy efficacy

In this section, we present a numerical investigation of a scenario where the infection source is at the center of the spatial domain (0.5, 0.5). The initial infection is concentrated within a circular area of a specified radius. A two-dimensional spatiotemporal simulation over an 8-month period is implemented using COMSOL Multiphysics.

Figure 2 illustrates that in the absence of control measures, the concentration of *V. cholerae P* diffuses from the central area towards the right side, eventually covering the domain. The spatial density distribution of infected individuals I increases synchronously, culminating in a full-scale outbreak.

To verify the effectiveness of regional control, a circular control area encompassing the infection source is defined. Figures 2 and 4 display the outcomes without control measures and with public health campaigns u_1 alone, respectively. Figure 4 indicates that the average infection density across the entire domain is significantly reduced compared to the uncontrolled scenario. However, infection control within the central area remains inadequate, and the infection density distribution on the right side exhibits a clear upward trend. Notably, the concentration of *V. cholerae* in the central area increases dramatically from the first to the eighth month (Figures 4(f)–(j)), confirming the limitations of a single-intervention strategy.

Following the introduction of the combined regional control strategy (u_2: vaccine expansion; u_3: water chlorination; u_4: intensive treatment), Figure 5 reveals a multi-ring gradient distribution pattern: each state variable increases radially from the center of the control area towards the periphery. By the each month, the infection density within the central control zone is maintained at a very low level, while densities in the uncontrolled peripheral areas do not exceed a moderate threshold. Comparative analysis demonstrates that the spatial density of infected individuals and the concentration of *V. cholerae* within the control area are markedly lower than those in the periphery, while the proportion of recovered individuals increases correspondingly.

Consistent with our findings, Chen et al. [31] observed that central outbreak scenarios lead to faster and more severe spatial spread compared to boundary-initiated outbreaks in schistosomiasis models. Their simulations further demonstrate that optimal regional control centered on the infection source significantly reduces infected human and snail populations, while accelerating recovery. This radial containment effect supports the strategic placement of control regions near high-risk diffusion cores, rather than at the periphery, to maximize intervention impact and minimize resource waste.

A comparison of *V. cholerae* concentrations between Figures 4 and 5 further corroborates the efficacy of regional control. In the sixth month, the pathogen concentration in the core area under combined control remains substantially lower than that observed in the peripheral areas under the single-control strategy. By the eighth month, the concentration in the outbreak area is suppressed to a minimal level, whereas the central area concentration under the single-control strategy reaches an extremely high value. This demonstrates that regional control plays a decisive role in blocking the dissemination of environmental pathogens.

Furthermore, we explore the cost constraints of different control strategies and comprehensively evaluate the overall efficacy of interventions in terms of epidemiological benefits (suppressing infected hosts I and environmental pathogens P) and control costs (J). As shown in Table 2, numerical simulation results indicate that single or partial intervention strategies exhibit significant limitations. Compared to the no-intervention strategy (S4), if only global early warning (S2, u_1) is adopted, the disease intervention effect is minimal due to the lack of substantive transmission-blocking measures. Conversely, if only the regional control strategy (S3, encompassing vaccination u_2, environmental disinfection u_3, and intensive treatment u_4) is implemented, although disease spread can be effectively curbed, such "passive response" excessively consumes public health resources. This leads to prohibitively high economic costs ($J_3 \approx 1484$), rendering it unfeasible for long-term execution. In contrast, the comprehensive control strategy (S1) demonstrates an outstanding synergistic optimization effect. This strategy effectively combines global early warning (u_1) with regional medical and disinfection interventions (u_2, u_3, u_4). The early warning mechanism effectively reduces the exposure base of the susceptible population in the initial stage of transmission, cutting off the exponential transmission chain at the source. Consequently, this greatly reduces the system's subsequent reliance on expensive vaccines, heavy disinfection, and clinical treatment resources. Therefore, this comprehensive strategy not only achieves the optimal epidemiological suppression effect ($U_3 \approx 343, U_5 \approx 2.96 \times 10^5$) but also dramatically minimizes the total control cost ($J_1 \approx 5.16$).

In summary, when responding to infectious diseases characterized by environmental transmission, an integrated comprehensive intervention scheme serves as the optimal decision-making paradigm. Adhering to early prevention investments at a minimal cost can significantly prevent downstream resource depletion and exorbitant expenditures, thereby achieving a global optimal balance between public health benefits and economic feasibility.

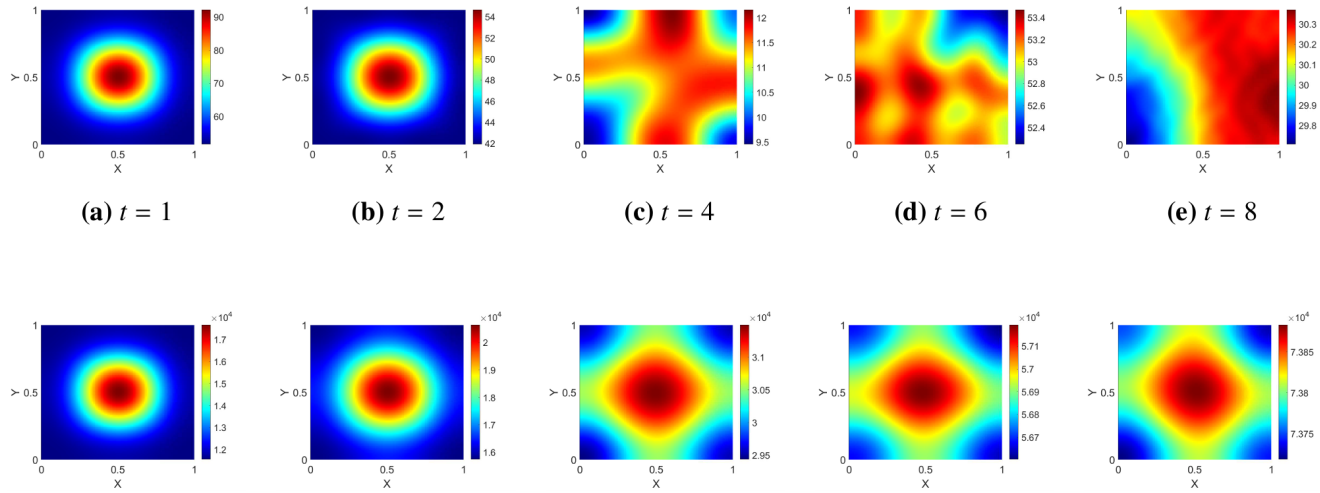

(a) $t = 1$ **(b)** $t = 2$ **(c)** $t = 4$ **(d)** $t = 6$ **(e)** $t = 8$

(f) $t = 1$ **(g)** $t = 2$ **(h)** $t = 4$ **(i)** $t = 6$ **(j)** $t = 8$

Figure 4. Evolution dynamics of I (top row) and P (bottom row) with u_1 and without u_2, u_3, and u_4.

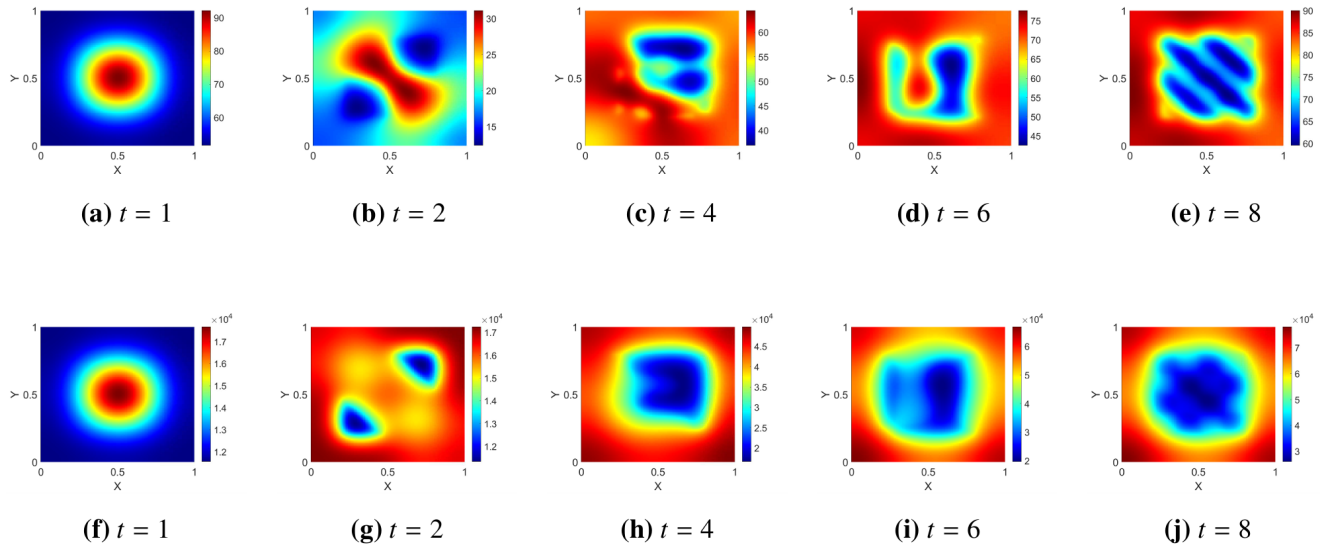

(a) $t = 1$ **(b)** $t = 2$ **(c)** $t = 4$ **(d)** $t = 6$ **(e)** $t = 8$

(f) $t = 1$ **(g)** $t = 2$ **(h)** $t = 4$ **(i)** $t = 6$ **(j)** $t = 8$

Figure 5. Evolution dynamics of I (top row) and P (bottom row) with u_2, u_3, and u_4 and without control of u_1.

Table 2. Comparison of epidemiological effects and costs under different control strategies.

Strategy	Total new infections (I)	Total new pathogens (P)	Total Cost (J)
S_1 (Comprehensive control)	343.18	296,044.68	5.16
S_2 (Global early warning)	492.06	1,071,326.68	30.54
S_3 (Regional control)	344.25	296,596.33	1,483.95
S_4 (No intervention)	499.65	1,079,360.88	0

5.2. Impact of initial spatial distribution on control efficacy

The spatial distribution of the initial infection source is a critical determinant of control effectiveness. In this subsection, we compare the dynamic responses under the combined control strategy (u_1, u_2, u_3, u_4) for central (as shown in Figure 6) and boundary outbreak (as shown in Figure 7) scenarios where $\chi_A(x, y) := [0, 0.4] \times [0.6, 1]$.

Numerical simulations show that when a cholera outbreak originates in the northwest corner of the spatial domain, the spatial density of infected individuals within the control area decreases by approximately half by the eighth month. Concurrently, a pronounced gradient in *V. cholerae* concentration is observed at the control boundary: The pathogen concentration within the controlled zone increases only slightly, while in the adjacent uncontrolled area, it surges dramatically from its initial level. This phenomenon underscores the significant impact of control area placement, with the pathogen flux reaching levels several times higher than those observed in the central outbreak scenario.

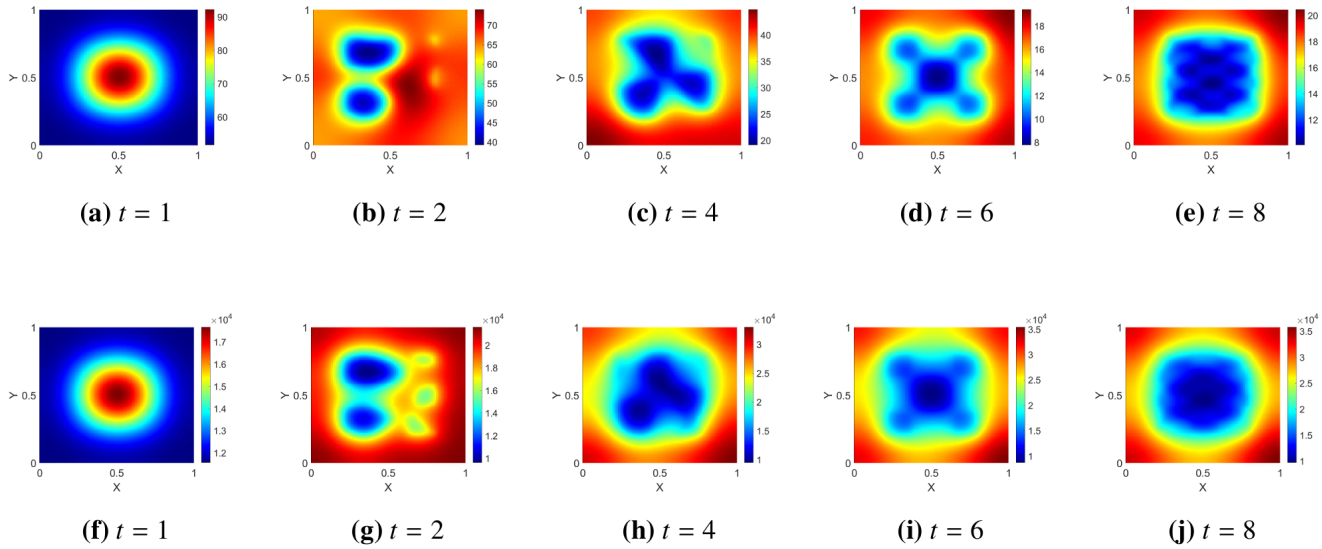

(a) $t = 1$ **(b)** $t = 2$ **(c)** $t = 4$ **(d)** $t = 6$ **(e)** $t = 8$

(f) $t = 1$ **(g)** $t = 2$ **(h)** $t = 4$ **(i)** $t = 6$ **(j)** $t = 8$

Figure 6. Evolution dynamics of I (top row) and P (bottom row) with u_1, u_2, u_3, and u_4.

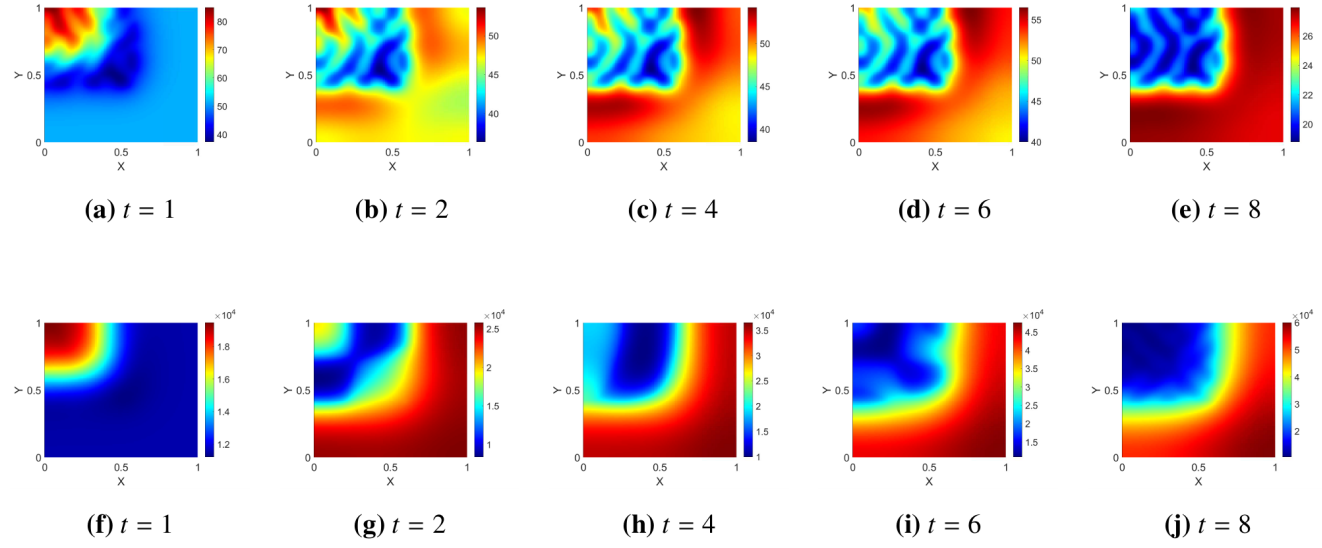

(a) $t = 1$ **(b)** $t = 2$ **(c)** $t = 4$ **(d)** $t = 6$ **(e)** $t = 8$

(f) $t = 1$ **(g)** $t = 2$ **(h)** $t = 4$ **(i)** $t = 6$ **(j)** $t = 8$

Figure 7. Evolution dynamics of I (top row) and P (bottom row) with u_1, u_2, u_3, and u_4 in the top left areas.

In contrast, the central outbreak scenario exhibits a distinct radial propagation pattern. During the initial stage, three discrete, low-infection-density rings form around the outer periphery of the infection core. As control measures continue, these ring structures coalesce into a continuous suppression belt by the third month and expand into a single, large ring structure by the eighth month, representing a substantial increase in the controlled area. The formation of this ring-shaped suppression belt results in a drastic reduction of *V. cholerae* concentration in the core area, which is markedly better than the reduction achieved in the boundary outbreak scenario. This indicates that the radial symmetry of a central outbreak significantly enhances the rate of infection density decay and shortens the time to the epidemic peak compared to a boundary outbreak.

The comparison of these results confirms the profound impact of the initial outbreak location and control area selection on the efficacy of control measures: Boundary outbreaks necessitate enhanced isolation protocols, whereas central outbreaks benefit from the expansion of radial suppression structures.

In addition, we further investigate the sensitivity of the optimal control results to spatial diffusion coefficients and disease transmission functions. Specifically, we vary the diffusion coefficient ($D = D_S = D_V = D_I = D_R = D_P$) and the transmission rate ($\beta := \beta_1, \beta_2$), comparing the temporal evolution of the total control intensity ($\int_\Omega \sum u_i(x, y, t)\, dx\, dy$) across scenarios. Numerical simulations reveal that the optimal control strategy exhibits a rational, adaptive sensitivity to both parameters:

(i) Sensitivity to the diffusion coefficient: An enlarged diffusion coefficient accelerates the spatially heterogeneous spread of hosts and pathogens, broadening the epidemic's scope. Consequently, the system is forced to trigger the peak total control intensity at an earlier stage and expand the spatial coverage of interventions to counteract rapid dissemination. Conversely, under low diffusion conditions, the control intensity remains milder and localized, as shown in Figures 8–10.

(ii) Sensitivity to the transmission function: An elevated transmission rate (β) significantly amplifies the disease's outbreak potential. This correspondingly raises the peak of the total control curve and notably prolongs the duration of high-intensity interventions, as shown in Figure 11. The system mitigates this heightened infection risk by increasing the overall input in both early warning (u_1) and subsequent medical treatment and disinfection (u_2, u_3, u_4). Although the absolute magnitude of the control intensity and the timing of the peak fluctuate with parameter variations, the overarching synergistic trend and morphological characteristics of the four integrated interventions remain consistent.

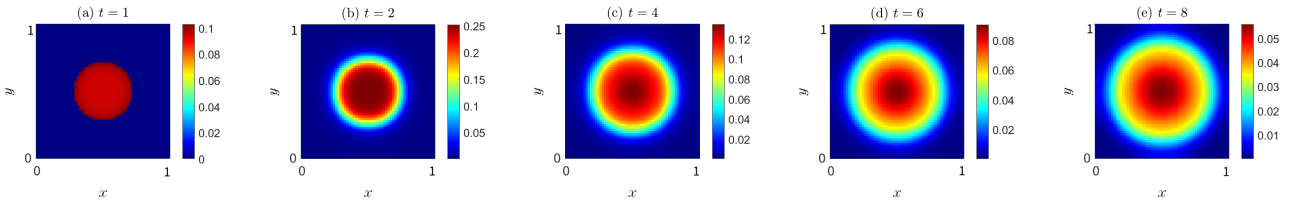

Figure 8. Spatiotemporal evolution of the total control intensity $u = \sum u_i(x, y, t)$ under $D = D_S = D_V = D_I = D_R = D_P = 0.1$.

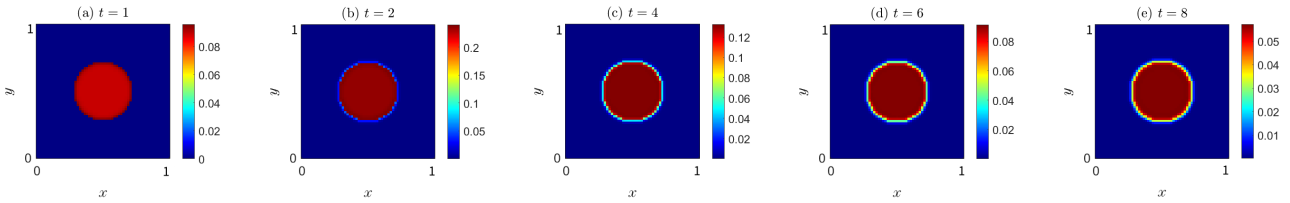

Figure 9. Spatiotemporal evolution of the total control intensity $u = \sum u_i(x, y, t)$ under $D = D_S = D_V = D_I = D_R = D_P = 0.001$.

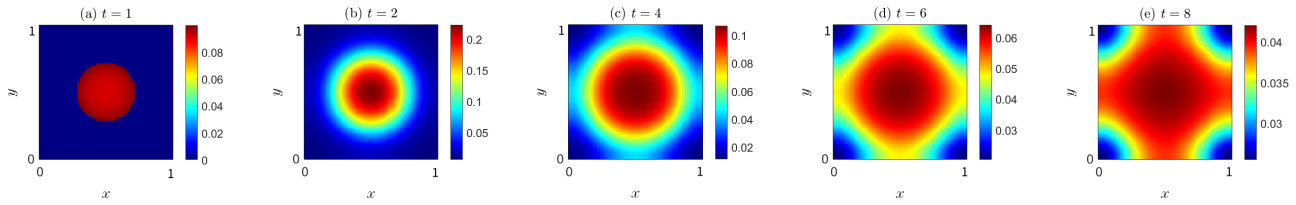

Figure 10. Spatiotemporal evolution of the total control intensity $u = \sum u_i(x, y, t)$ under $D = D_S = D_V = D_I = D_R = D_P = 0.5$.

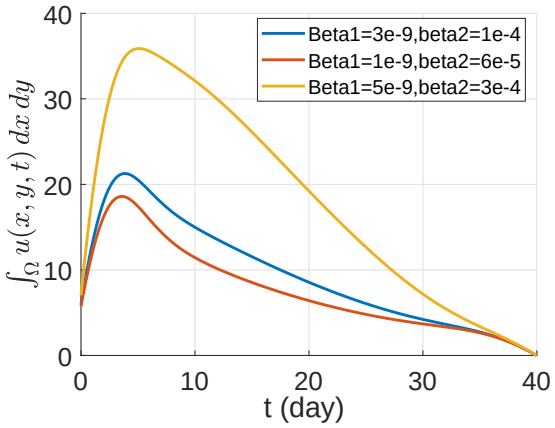

Figure 11. Temporal evolution of the spatially integrated total control intensity $u = \sum u_i(x, y, t)$ under varying propagation coefficients.

6. Conclusions

In this study, we address the core challenges in cholera control, namely, the low coverage, high cost, and sub-optimal effectiveness of traditional uniform strategies stemming from spatial heterogeneity, by pioneering a regional optimal-control framework based on reaction-diffusion equations. The model quantifies the directional dispersal dynamics of pathogens along river networks to identify high-risk sub-domains and proposes an innovative four-dimensional intervention strategy that synergistically integrates population-wide health education with targeted sub-domain measures (vaccine expansion, water chlorination, and case isolation), forming a closed-loop prevention-blocking-elimination system.

Building upon the proposed model, its rationality and validity are rigorously demonstrated at the theoretical level. The analysis establishes the existence, uniqueness, non-negativity, and boundedness of strong solutions for the controlled system, ensuring its mathematical soundness. Furthermore, the necessary optimality conditions for the control functions are derived using Pontryagin's maximum principle, providing a solid theoretical foundation for numerically determining the optimal strategies.

To validate the practical effectiveness of this theoretical model, systematic comparative experiments are conducted via numerical simulations and a control-variable approach. The results demonstrate that the regional combined-control strategy significantly outperforms no control or single interventions: It maintains infection density at a very low level in the core zone, substantially reduces *V.*

cholerae concentration within a short period, markedly lowers secondary-outbreak risk, and achieves considerably higher resource efficiency than uniform strategies. Spatio-temporal dynamics further reveal a significant expansion of radial suppression zones around central outbreaks, whose control efficacy surpasses that of boundary-outbreak scenarios, conclusively proving the significant advantage of targeted regional interventions.

Despite the promising results, this study has certain limitations. Primarily, the parameters utilized in the numerical simulations are derived from the literature rather than calibrated against specific real-world epidemiological datasets, which constrains the model's immediate practical deployment. Furthermore, the current framework does not precisely quantify the absolute economic benefits of the proposed strategy; its cost-effectiveness is reflected only through relative-efficiency metrics, lacking a universal quantitative standard for the degree of improvement. Additionally, our model assumes homogeneous Neumann boundary conditions, which biologically neglects cross-border population and pathogen mobility. Incorporating alternative boundary conditions to reflect open environments introduces significant mathematical complexities into the optimal control framework, making it a challenging topic for our future research.

To address these limitations, in future work, we will focus on calibrating the model using real epidemiological data, integrating health-economic analysis frameworks to thoroughly quantify cost-benefit and cost-utility, and translating the model outputs into precise, actionable public-health indicators to enhance the framework's real-world applicability.

Use of AI tools declaration

The authors declare they have not used Artificial Intelligence (AI) tools in the creation of this article.

Acknowledgments

The work is partially supported by the National Natural Science Foundation of China (No.12201557), the Fundamental Research Funds for the Provincial Universities of Zhejiang (No. GK249909299001-020).

Conflict of interest

The authors declare there are no conflicts of interest.

Data availability

Data come from published resources. The programs for the simulations can be found at https://github.com/dudududuroududu/Optimal-Regional-Cholera-Control.

References

1. D. A. Sack, R. B. Sack, G. B. Nair, A. K. Siddique, Cholera, *Lancet*, **363** (2004), 223–233. https://doi.org/10.1016/S0140-6736(03)15328-7

2. J. B. Harris, R. C. LaRocque, F. Qadri, E. T. Ryan, S. B. Calderwood, Cholera, *Lancet*, **379** (2012), 2466–2476. https://doi.org/10.1016/S0140-6736(12)60436-X

3. D. Barua, History of cholera, *Cholera*, (1992), 1–36. https://doi.org/10.1007/978-1-4757-9688-9_1

4. M. Ali, A. R. Nelson, A. L. Lopez, D. A. Sack, Updated global burden of cholera in endemic countries, *PLoS Negl.Trop. Dis.*, **9** (2015), e0003832. https://doi.org/10.1371/journal.pntd.0003832

5. World Health Organization, Cholera – Global situation, in *Disease Outbreak News*, 2023. Available from: https://www.who.int/emergencies/disease-outbreak-news/item/2023-DON437.

6. A. Camacho, M. Bouhenia, R. Alyusfi, A. Alkohlani, M. A. M. Naji, X. Radiguès, et al., Cholera epidemic in Yemen, 2016–18: an analysis of surveillance data, *Lancet Global Health*, **6** (2018), e680–e690. https://doi.org/10.1016/S2214-109X(18)30230-4

7. V. Capasso, S. L. Paveri-Fontana, A mathematical model for the 1973 cholera epidemic in the European Mediterranean region, *Rev. Epidemiol. Sante Publique*, **27** (1979), 121–132.

8. A. S. Azman, K. E. Rudolph, D. A. T. Cummings, J. Lessler, The incubation period of cholera: a systematic review, *J. Infect.*, **66** (2013), 432–438. https://doi.org/10.1016/j.jinf.2012.11.013

9. C. T. Codeço, Endemic and epidemic dynamics of cholera: the role of the aquatic reservoir, *BMC Infect. Dis.*, **1** (2001), 1. https://doi.org/10.1186/1471-2334-1-1

10. H. Zhao, S. Zou, X. Wang, Y. Chen, Dynamic behaviors of a cholera model with nonlinear incidences, multiple transmission pathways, and imperfect vaccine, *J. Appl. Math. Comput.*, **70** (2024), 917–946. https://doi.org/10.1007/s12190-024-01994-9

11. Z. Mukandavire, S. Liao, J. Wang, H. Gaff, D. L. Smith, J. G. Morris, Estimating the reproductive numbers for the 2008–2009 cholera outbreaks in Zimbabwe, *Proc. Natl. Acad. Sci. U.S.A.*, **108** (2011), 8767–8772. https://doi.org/10.1073/pnas.1019712108

12. X. Tian, R. Xu, J. Lin, Mathematical analysis of a cholera infection model with vaccination strategy, *Appl. Math. Comput.*, **361** (2019), 517–535. https://doi.org/10.1016/j.amc.2019.05.055

13. J. Wang, F. Xie, T. Kuniya, Analysis of a reaction-diffusion cholera epidemic model in a spatially heterogeneous environment, *Commun. Nonlinear Sci. Numer. Simul.*, **80** (2020), 104951. https://doi.org/10.1016/j.cnsns.2019.104951

14. M. A. Safi, D. Y. Melesse, A. B. Gumel, Dynamics analysis of a multi-strain cholera model with an imperfect vaccine, *Bull. Math. Biol.*, **75** (2013), 1104–1137. https://doi.org/10.1007/s11538-013-9845-2

15. X. Wang, X. Q. Zhao, J. Wang, A cholera epidemic model in a spatiotemporally heterogeneous environment, *J. Math. Anal. Appl.*, **468** (2018), 893–912. https://doi.org/10.1016/j.jmaa.2018.08.039

16. F. Capone, V. Cataldis, R. De Luca, Influence of diffusion on the stability of equilibria in a reaction-diffusion system modeling cholera dynamics, *J. Math. Biol.*, **71** (2015), 1107–1131. https://doi.org/10.1007/s00285-014-0849-9

17. X. Wang, D. Posny, J. Wang, A reaction-convection-diffusion model for cholera spatial dynamics, *Discrete Contin. Dyn. Syst. - Ser. B*, **21** (2016), 2785–2809. https://doi.org/10.3934/dcdsb.2016073

18. E. Bertuzzo, R. Casagrandi, M. Gatto, I. Rodriguez-Iturbe, A. Rinaldo, On spatially explicit models of cholera epidemics, *J. R. Soc. Interface*, **7** (2009), 321–333. https://doi.org/10.1098/rsif.2009.0204

19. N. Bai, C. Song, R. Xu, Mathematical analysis and application of a cholera transmission model with waning vaccine-induced immunity, *Nonlinear Anal. Real World Appl.*, **58** (2021), 103232. https://doi.org/10.1016/j.nonrwa.2020.103232

20. C. Modnak, A model of cholera transmission with hyperinfectivity and its optimal vaccination control, *Int. J. Biomath.*, **10** (2017), 1750084. https://doi.org/10.1142/S179352451750084X

21. Y. Kang, L. Nie, Dynamical analysis and optimal control of an age-structured epidemic model with asymptomatic infection and multiple transmission pathways, *Math. Methods Appl. Sci.*, **47** (2024), 9669–9702. https://doi.org/10.1002/mma.10088

22. W. Li, L. Zhang, J. Cao, F. Xu, Z. Cai, Finite time attractivity and exponentially stable of a multistage epidemic system with discontinuous incidence, *Qual. Theory Dyn. Syst.*, **24** (2025), 199. https://doi.org/10.1007/s12346-025-01358-z

23. M. S. Islam, M. A. Miah, M. K. Hasan, R. B. Sack, M. J. Albert Detection of non-culturable *Vibrio cholerae* O1 associated with a cyanobacterium from an aquatic environment in Bangladesh, *Trans. R. Soc. Trop. Med. Hyg.*, **88** (1994), 298–299. https://doi.org/10.1016/0035-9203(94)90085-X

24. D. Lantagne, T. Yates, Household water treatment and cholera control, *J. Infect. Dis.*, **218** (2018), S147–S153. https://doi.org/10.1093/infdis/jiy488

25. F. Qadri, M. Ali, J. Lynch, F. Chowdhury, A. I. Khan, T. F. Wierzba, et al., Efficacy of a single-dose regimen of inactivated whole-cell oral cholera vaccine: results from 2 years of follow-up of a randomised trial, *Lancet Infect. Dis.*, **18** (2018), 666–674. https://doi.org/10.1016/S1473-3099(18)30108-7

26. K. Sévère, V. Rouzier, S.B. Anglade, et al., Effectiveness of oral cholera vaccine in Haiti: 37-month follow-up, *Am. J. Trop. Med. Hyg.*, **94** (2016), 1136. https://doi:10.4269/ajtmh.15-0700

27. S. Zhang, S. Fan, P. Wu, Complete dynamics of a heterogeneous space diffusion cholera model with nonlocal time delay and drug resistance, *Z. Angew. Math. Phys.*, **76** (2025), 200. https://doi.org/10.1007/s00033-025-02584-w

28. W. Wang, X. Wang, H. Wang, Spatial dynamics of a generalized cholera model with nonlocal time delay in a heterogeneous environment, *J. Differ. Equations*, **405** (2024), 103–150. https://doi.org/10.1016/j.jde.2024.05.049

29. W. Li, L. Yang, J. Cao, Threshold dynamics of a degenerated diffusive incubation period host–pathogen model with saturation incidence rate, *Appl. Math. Lett.*, **160** (2025), 109312. https://doi.org/10.1016/j.aml.2024.109312

30. A. El A. Laaroussi, M. Rachik, On the regional control of a reaction-diffusion system SIR, *Bull. Math. Biol.*, **82** (2020), 5. https://doi.org/10.1007/s11538-019-00673-2

31. T. Chen, L. Chen, P. Wu, Spatiotemporal transmission dynamics and optimal regional control of a spatial heterogeneity reaction-diffusion schistosomiasis model, *Commun. Nonlinear Sci. Numer. Simul.*, **151** (2025), 109097. https://doi.org/10.1016/j.cnsns.2025.109097

Appendix

H^* is the adjoint matrix provided in the Appendix, which serves as the coefficient matrix of the adjoint system derived via Pontryagin's maximum principle in the optimal control problem. This matrix incorporates information from the state variables and control variables, and is utilized for numerically solving the optimal control strategy. Due to the complexity of the matrix expression and its inclusion of cross-terms involving multiple state and control variables, it is placed in the appendix to maintain the conciseness of the main text.

$$H^* = \begin{pmatrix} H_{11} & H_{12} & H_{13} & H_{14} & H_{15} \\ H_{21} & H_{22} & H_{23} & H_{24} & H_{25} \\ H_{31} & H_{32} & H_{33} & H_{34} & H_{35} \\ H_{41} & H_{42} & H_{43} & H_{44} & H_{45} \\ H_{51} & H_{52} & H_{53} & H_{54} & H_{55} \end{pmatrix}$$

$$\begin{aligned}
H_{11} &= -\mu\Big[(-\mu w_5 - u_3 w(x,y))[(-I\beta_2\sigma - \eta - \mu - \beta_1 w_5\sigma)(-\gamma - \delta_I - \mu + \beta_2 w_1 + \beta_2\sigma w_2) \\
&\quad + \beta_2\sigma w_2(\beta_1 w_5\sigma + I\beta_2\sigma) - \xi(\beta_1^2(-w_5)\sigma w_1 - I\beta_1\beta_2\sigma w_1 - \beta_1\eta w_1 - \beta_1\mu w_1 - \beta_1\eta\sigma w_2 - \beta_1\mu\sigma w_2)]\Big] \\
H_{12} &= \mu\Big[(-\mu w_5 - u_3 w(x,y))(-\gamma\eta - \delta_I\eta - \eta\mu + \beta_1\beta_2 w_5\sigma w_1 + I\beta_2^2\sigma w_1 + \beta_2\eta w_1 + \beta_2\eta\sigma w_2) \\
&\quad - \xi(\beta_1^2 w_5\sigma w_1 + I\beta_1\beta_2\sigma w_1 + \beta_1\eta w_1 + \beta_1\eta\sigma w_2)\Big] \\
H_{13} &= \beta_1^2\mu\xi(-w_5)\sigma w_1 - \beta_1\beta_2\mu^2 w_5\sigma w_1 - \beta_1\beta_2\mu w_5\sigma w_1 u_3 w(x,y) - I\beta_1\beta_2\mu\xi\sigma w_1 - \beta_1\eta\mu\xi w_1 \\
&\quad - \beta_1\mu^2\xi w_1 - I\beta_2^2\mu^2 w_5\sigma w_1 - \beta_2\eta\mu^2 w_5 w_1 - \beta_2\mu^3 w_5 w_1 - I\beta_2^2\mu\sigma w_1 u_3 w(x,y) \\
&\quad - \beta_2\eta\mu w_1 u_3 w(x,y) - \beta_2\mu^2 w_1 u_3 w(x,y) - \beta_2\eta\mu\sigma u_3 w_2 w(x,y) - \beta_1\eta\mu\xi\sigma w_2 - \beta_2\eta\mu^2 w_5\sigma w_2 \\
H_{14} &= 0 \\
H_{15} &= -\beta_1^2\gamma\mu w_5\sigma w_1 - \beta_1^2\delta_I\mu w_5\sigma w_1 - \beta_1^2\mu^2 w_5\sigma w_1 - I\beta_1\beta_2\gamma\mu\sigma w_1 - I\beta_1\beta_2\delta_I\mu\sigma w_1 \\
&\quad - I\beta_1\beta_2\mu^2\sigma w_1 - \beta_1\gamma\eta\mu w_1 - \beta_1\gamma\mu^2 w_1 - \beta_1\delta_I\eta\mu w_1 - \beta_1\delta_I\mu^2 w_1 - \beta_1\eta\mu^2 w_1 \\
&\quad - \beta_1\gamma\eta\mu\sigma w_2 - \beta_1\delta_I\eta\mu\sigma w_2 - \beta_1\eta\mu^2\sigma w_2 \\
H_{21} &= \mu\Big[(-\mu w_5 - u_3 w(x,y))[(u_2 w(x,y) + \Phi)(-\gamma - \delta_I - \mu + \beta_2 w_1 + \beta_2\sigma w_2) + \beta_2\sigma w_2(\beta_1 w_5 + I\beta_2)] \\
&\quad - \xi(\beta_1^2 w_5\sigma w_2 + \beta_1 w_1\Phi + \beta_1 w_1 u_2 w(x,y) + \beta_1\sigma u_2 w_2 w(x,y) + I\beta_1\beta_2\sigma w_2 + \beta_1\sigma w_2\Phi)\Big] \\
H_{22} &= -\mu\Big[(-\mu w_5 - u_3 w(x,y))[\beta_2 w_1(\beta_1 w_5 + I\beta_2) + (-\gamma - \delta_I - \mu + \beta_2 w_1 + \beta_2\sigma w_2)(-I\beta_2 - \mu - \beta_1 w_5 \\
&\quad - u_1 - u_2 w(x,y) - \Phi)] - \xi(\beta_1^2(-w_5)\sigma w_2 - \beta_1\mu w_1 - \beta_1 w_1\Phi - \beta_1 w_1 u_1 - \beta_1 w_1 u_2 w(x,y) \\
&\quad - \beta_1\sigma u_1 w_2 - \beta_1\sigma u_2 w_2 w(x,y) - I\beta_1\beta_2\sigma w_2 - \beta_1\mu\sigma w_2 - \beta_1\sigma w_2\Phi)\Big] \\
H_{23} &= \mu\Big[(-\mu w_5 - u_3 w(x,y))[\beta_1\beta_2 w_5\sigma w_2 + \beta_2 w_1\Phi + \beta_2 w_1 u_2 w(x,y) + \beta_2\sigma u_1 w_2 + \beta_2\sigma u_2 w_2 w(x,y) \\
&\quad + I\beta_2^2\sigma w_2 + \beta_2\mu\sigma w_2 + \beta_2\sigma w_2\Phi] - \xi(\beta_1^2 w_5\sigma w_2 + \beta_1 w_1\Phi + \beta_1 w_1 u_2 w(x,y) + \beta_1\sigma u_1 w_2 \\
&\quad + \beta_1\sigma u_2 w_2 w(x,y) + I\beta_1\beta_2\sigma w_2 + \beta_1\mu\sigma w_2 + \beta_1\sigma w_2\Phi)\Big] \\
H_{24} &= 0 \\
H_{25} &= -\beta_1^2\gamma\mu w_5\sigma w_2 - \beta_1^2\delta_I\mu w_5\sigma w_2 - \beta_1^2\mu^2 w_5\sigma w_2 - \beta_1\gamma\mu w_1\Phi - \beta_1\delta_I\mu w_1\Phi - \beta_1\mu^2 w_1\Phi \\
&\quad - \beta_1\gamma\mu w_1 u_2 w(x,y) - \beta_1\delta_I\mu w_1 u_2 w(x,y) - \beta_1\mu^2 w_1 u_2 w(x,y) - \beta_1\gamma\mu\sigma u_1 w_2 - \beta_1\delta_I\mu\sigma u_1 w_2 - \beta_1\mu^2\sigma u_1 w_2 \\
&\quad - \beta_1\gamma\mu\sigma u_2 w_2 w(x,y) - \beta_1\delta_I\mu\sigma u_2 w_2 w(x,y) - \beta_1\mu^2\sigma u_2 w_2 w(x,y) - I\beta_1\beta_2\gamma\mu\sigma w_2 - I\beta_1\beta_2\delta_I\mu\sigma w_2
\end{aligned}$$

$$
\begin{aligned}
&- I\beta_1\beta_2\mu^2\sigma w_2 - \beta_1\gamma\mu^2\sigma w_2 - \beta_1\gamma\mu\sigma w_2\Phi - \beta_1\delta_I\mu^2\sigma w_2 - \beta_1\delta_I\mu\sigma w_2\Phi - \beta_1\mu^3\sigma w_2 - \beta_1\mu^2\sigma w_2\Phi\\
H_{31} &= (-\mu w_5 - u_3 w(x,y))[\beta_2^2\mu\sigma - I\beta_2\eta\mu - I\beta_2\mu^2 - I\beta_2\mu\sigma\Phi + \beta_1^2\mu(-w_5^2)\sigma - 2I\beta_1\beta_2\mu w_5\sigma\\
&\quad - \beta_1\eta\mu w_5 - \beta_1\mu^2 w_5 - \beta_1\mu w_5\sigma\Phi - \beta_1\mu w_5\sigma u_2 w(x,y) - I\beta_2\mu\sigma u_2 w(x,y)]\\
H_{32} &= \mu(-\mu w_5 - u_3 w(x,y))[(\beta_1 w_5\sigma + I\beta_2\sigma)(-I\beta_2 - \mu - \beta_1 w_5 - u_1 - u_2 w(x,y) - \Phi) - \eta(\beta_1 w_5 + I\beta_2)]\\
H_{33} &= -\mu(-\mu w_5 - u_3 w(x,y))[-\eta(u_2 w(x,y) + \Phi) + (-I\beta_2\sigma - \eta - \mu - \beta_1 w_5\sigma)(-I\beta_2 - \mu - \beta_1 w_5 - u_1\\
&\quad - u_2 w(x,y) - \Phi)]\\
H_{34} &= 0\\
H_{35} &= \beta_1^2\mu^2 w_5\sigma w_1 + \beta_1^2\mu w_5\sigma w_1 u_1 + \beta_1^2\mu^2 w_5\sigma w_2 + I\beta_1\beta_2\mu^2\sigma w_1 + \beta_1\eta\mu^2 w_1 + \beta_1\mu^3 w_1 + \beta_1\mu^2 w_1\Phi\\
&\quad + I\beta_1\beta_2\mu\sigma w_1 u_1 + \beta_1\eta\mu w_1 u_1 + \beta_1\mu^2 w_1 u_1 + \beta_1\mu^2 w_1 u_2 w(x,y) + \beta_1\eta\mu\sigma u_1 w_2 + \beta_1\mu^2\sigma u_1 w_2\\
&\quad + \beta_1\mu^2\sigma u_2 w_2 w(x,y) + I\beta_1\beta_2\mu^2\sigma w_2 + \beta_1\eta\mu^2\sigma w_2 + \beta_1\mu^3\sigma w_2 + \beta_1\mu^2\sigma w_2\Phi\\
H_{41} &= \xi[\beta_1^2(-w_5)\sigma w_1 u_1 - I\beta_1\beta_2\sigma w_1 u_1 - \beta_1\eta w_1 u_1 - \beta_1\mu w_1 u_1 - \beta_1\eta\sigma u_1 w_2 - \beta_1\mu\sigma u_1 w_2]\\
&\quad - (-\mu w_5 - u_3 w(x,y))[\gamma(\beta_2^2\sigma - I\beta_2\eta - I\beta_2\mu - I\beta_2\sigma\Phi - \beta_1^2 w_5^2\sigma - 2I\beta_1\beta_2 w_5\sigma - \beta_1\eta w_5\\
&\quad - \beta_1\mu w_5 - \beta_1 w_5\sigma\Phi - \beta_1 w_5\sigma u_2 w(x,y) - I\beta_2\sigma u_2 w(x,y)) + u_1((-I\beta_2\sigma - \eta - \mu - \beta_1 w_5\sigma)\\
&\quad \cdot(-\gamma - \delta_I - \mu + \beta_2 w_1 + \beta_2\sigma w_2) + \beta_2\sigma w_2(\beta_1 w_5\sigma + I\beta_2\sigma))]\\
H_{42} &= (-\mu w_5 - u_3 w(x,y))[u_1(-\gamma\eta - \delta_I\eta - \eta\mu + \beta_1\beta_2 w_5\sigma w_1 + I\beta_2^2\sigma w_1 + \beta_2\eta w_1 + \beta_2\eta\sigma w_2)\\
&\quad + \gamma((\beta_1 w_5\sigma + I\beta_2\sigma)(-I\beta_2 - \mu - \beta_1 w_5 - u_1 - u_2 w(x,y) - \Phi) - \eta(\beta_1 w_5 + I\beta_2))]\\
&\quad - \xi[\beta_1^2 w_5\sigma w_1 u_1 + I\beta_1\beta_2\sigma w_1 u_1 + \beta_1\eta w_1 u_1 + \beta_1\eta\sigma u_1 w_2]\\
H_{43} &= \xi[\beta_1^2(-w_5)\sigma w_1 u_1 - I\beta_1\beta_2\sigma w_1 u_1 - \beta_1\eta w_1 u_1 - \beta_1\mu w_1 u_1 - \beta_1\eta\sigma u_1 w_2]\\
&\quad - (-\mu w_5 - u_3 w(x,y))[u_1(-\beta_1\beta_2 w_5\sigma w_1 - I\beta_2^2\sigma w_1 - \beta_2\eta w_1 - \beta_2\mu w_1 - \beta_2\eta\sigma w_2)\\
&\quad + \gamma(-\eta(u_2 w(x,y) + \Phi) + (-I\beta_2\sigma - \eta - \mu - \beta_1 w_5\sigma)(-I\beta_2 - \mu - \beta_1 w_5 - u_1 - u_2 w(x,y) - \Phi))]\\
H_{44} &= (-\mu w_5 - u_3 w(x,y))[-(\beta_1 w_5\sigma + I\beta_2\sigma)(\beta_1\beta_2 w_5\sigma w_2 + \beta_2 w_1\Phi + \beta_2 w_1 u_2 w(x,y) + \beta_2\sigma u_1 w_2\\
&\quad + \beta_2\sigma u_2 w_2 w(x,y) + I\beta_2^2\sigma w_2 + \beta_2\mu\sigma w_2 + \beta_2\sigma w_2\Phi) + (-\gamma - \delta_I - \mu + \beta_2 w_1 + \beta_2\sigma w_2)\\
&\quad \cdot(-\eta(u_2 w(x,y) + \Phi) + (-I\beta_2\sigma - \eta - \mu - \beta_1 w_5\sigma)(-I\beta_2 - \mu - \beta_1 w_5 - u_1 - u_2 w(x,y) - \Phi))\\
&\quad + (\beta_1 w_5 + I\beta_2)(-\beta_1\beta_2 w_5\sigma w_1 - I\beta_2^2\sigma w_1 - \beta_2\eta w_1 - \beta_2\mu w_1 - \beta_2\eta\sigma w_2)]\\
&\quad - \xi[\beta_1^2\mu w_5\sigma w_1 + \beta_1^2 w_5\sigma w_1 u_1 + \beta_1^2\mu w_5\sigma w_2 + I\beta_1\beta_2\mu\sigma w_1 + \beta_1\eta\mu w_1 + \beta_1\mu^2 w_1 + \beta_1\mu w_1\Phi\\
&\quad + I\beta_1\beta_2\sigma w_1 u_1 + \beta_1\eta w_1 u_1 + \beta_1\mu w_1 u_1 + \beta_1\mu w_1 u_2 w(x,y) + \beta_1\eta\sigma u_1 w_2 + \beta_1\mu\sigma u_1 w_2\\
&\quad + \beta_1\mu\sigma u_2 w_2 w(x,y) + I\beta_1\beta_2\mu\sigma w_2 + \beta_1\eta\mu\sigma w_2 + \beta_1\mu^2\sigma w_2 + \beta_1\mu\sigma w_2\Phi]\\
H_{45} &= \beta_1^2\gamma\mu w_5\sigma w_1 + \beta_1^2\delta_I(-w_5)\sigma w_1 u_1 - \beta_1^2\mu w_5\sigma w_1 u_1 + \beta_1^2\gamma\mu w_5\sigma w_2 + I\beta_1\beta_2\gamma\mu\sigma w_1\\
&\quad + \beta_1\gamma\eta\mu w_1 + \beta_1\gamma\mu^2 w_1 + \beta_1\gamma\mu w_1\Phi - I\beta_1\beta_2\delta_I\sigma w_1 u_1 - I\beta_1\beta_2\mu\sigma w_1 u_1 - \beta_1\delta_I\eta w_1 u_1\\
&\quad - \beta_1\delta_I\mu w_1 u_1 - \beta_1\eta\mu w_1 u_1 - \beta_1\mu^2 w_1 u_1 + \beta_1\gamma\mu w_1 u_2 w(x,y) + \beta_1\gamma\mu\sigma u_1 w_2 - \beta_1\delta_I\eta\sigma u_1 w_2\\
&\quad - \beta_1\eta\mu\sigma u_1 w_2 + \beta_1\gamma\mu\sigma u_2 w_2 w(x,y) + I\beta_1\beta_2\gamma\mu\sigma w_2 + \beta_1\gamma\eta\mu\sigma w_2 + \beta_1\gamma\mu^2\sigma w_2 + \beta_1\gamma\mu\sigma w_2\Phi\\
H_{51} &= -\beta_2^2\mu\xi\sigma + I\beta_2\eta\mu\xi + I\beta_2\mu^2\xi + I\beta_2\mu\xi\sigma\Phi + \beta_1^2\mu\xi w_5^2\sigma + 2I\beta_1\beta_2\mu\xi w_5\sigma + \beta_1\eta\mu\xi w_5\\
&\quad + \beta_1\mu^2\xi w_5 + \beta_1\mu\xi w_5\sigma\Phi + \beta_1\mu\xi w_5\sigma u_2 w(x,y) + I\beta_2\mu\xi\sigma u_2 w(x,y)\\
H_{52} &= -\mu\xi[(\beta_1 w_5\sigma + I\beta_2\sigma)(-I\beta_2 - \mu - \beta_1 w_5 - u_1 - u_2 w(x,y) - \Phi) - \eta(\beta_1 w_5 + I\beta_2)]\\
H_{53} &= \mu\xi[-\eta(u_2 w(x,y) + \Phi) + (-I\beta_2\sigma - \eta - \mu - \beta_1 w_5\sigma)(-I\beta_2 - \mu - \beta_1 w_5 - u_1 - u_2 w(x,y) - \Phi)]\\
H_{54} &= 0
\end{aligned}
$$

$$
\begin{aligned}
H_{55} = -\mu[&-(\beta_1 w_5\sigma + I\beta_2\sigma)(\beta_1\beta_2 w_5\sigma w_2 + \beta_2 w_1\Phi + \beta_2 w_1 u_2 w(x,y) + \beta_2\sigma u_1 w_2 + \beta_2\sigma u_2 w_2 w(x,y)\\
&+ I\beta_2^2\sigma w_2 + \beta_2\mu\sigma w_2 + \beta_2\sigma w_2\Phi) + (-\gamma - \delta_I - \mu + \beta_2 w_1 + \beta_2\sigma w_2)\\
&\cdot(-\eta(u_2 w(x,y) + \Phi) + (-I\beta_2\sigma - \eta - \mu - \beta_1 w_5\sigma)(-I\beta_2 - \mu - \beta_1 w_5 - u_1 - u_2 w(x,y) - \Phi))\\
&+ (\beta_1 w_5 + I\beta_2)(-\beta_1\beta_2 w_5\sigma w_1 - I\beta_2^2\sigma w_1 - \beta_2\eta w_1 - \beta_2\mu w_1 - \beta_2\eta\sigma w_2)]
\end{aligned}
$$

AIMS Press